ANL/MHD-78-2

MASTER

ANL/MHD-78-2

Office of Naval Research
Order No. N00014-77-F-0006
Task No. NR 099-404

Annual Report
October 1976 to September 1977

EXPERIMENTAL TWO-PHASE LIQUID-METAL MAGNETOHYDRODYNAMIC GENERATOR PROGRAM

by

M. Petrick, Project Scientist
G. Fabris
E. S. Pierson
A. K. Fischer
C. E. Johnson

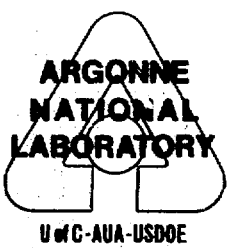

Engineering Division

May 1978

ANL/MHD-78-2

OFFICE OF NAVAL RESEARCH

ANNUAL REPORT

October 1976 to September 1977

EXPERIMENTAL TWO-PHASE LIQUID-METAL MAGNETOHYDRODYNAMIC GENERATOR PROGRAM

by

M. Petrick, Project Scientist

G. Fabris

E. S. Pierson

A. K. Fischer

C. E. Johnson

ENGINEERING DIVISION

May 1978

Approved for public release; distribution unlimited

TABLE OF CONTENTS

	Page
LIST OF FIGURES	v
LIST OF TABLES	vii
NOMENCLATURE	viii
DEFINITIONS	x
SUMMARY	1
I. INTRODUCTION	2
II. PROGRAM	5
II.1 NaK-N_2 Generator Experiments	5
II.2 Foams	5
II.3 Analytical Studies	7
II.3.1 Shunt Layer.	7
II.3.2 Pressure-Gradient Correlation	11
II.3.3 Imperfect Compensation	12
III. GENERATOR PERFORMANCE	16
III.1 Comparison with Previous Data	16
III.2 Influence of Flow Rate	20
III.2.1 Efficiency	20
III.2.2 Slip Ratio	22
III.3 Liquid-to-Gas Heat Transfer.	37
III.4 Magnetic Field Shaping	47
IV. LIQUID-METAL FOAMS AND SURFACE-ACTIVE AGENTS	49
IV.1 System Description and Experimental Approach	49
IV.1.1 Particle Dispersions	49
IV.1.2 Soluble Additives	51
IV.1.3 Experimental Approach	54
IV.2 Results	55
IV.2.1 Wetting Aspects	55
IV.2.2 Particulate Dispersion	59
IV.2.3 Soluble Additives	64

TABLE OF CONTENTS (Cont'd)

		Page
V.	CONCLUSIONS AND FUTURE WORK	71
V.1	Higher Velocities and Pressures	73
V.2	Foams	73
V.3	End Effects	75
V.4	Imperfect Compensation	75
V.5	Improved Local Diagnostics	76
REFERENCES		77
APPENDIX A	Summary of Experimental Generator Data, October 1977 to September 1978	79

LIST OF FIGURES

No.	Title	Page
I.1	Channel Contours Used in ANL LMMHD Generator Experiments	3
II.1	NaK-Nitrogen Flow Loop	6
II.2	Generator Efficiency vs. Load Factor for Various Hartmann Numbers	10
II.3	Comparison of Two-Phase MHD Pressure-Gradient Correlation with Ambient-Temperature NaK-N_2 Generator Data	13
III.1	Liquid Velocity Along Generator	19
III.2	Influence of Flow Rate on Generator Efficiency, B = 1.2 Tesla	21
III.3	Liquid Velocity Along Generator, $\dot{m}_\ell$ = 6 kg/s	23
III.4	Slip Ratio Along Generator, $\dot{m}_\ell$ = 6 kg/s	24
III.5	Pressure Along Generator, $\dot{m}_\ell$ = 6 kg/s	25
III.6	Local Load Factor Along Generator, $\dot{m}_\ell$ = 6 kg/s	26
III.7	Void Fraction Along Generator, $\dot{m}_\ell$ = 6 kg/s	27
III.8	Liquid Velocity Along Generator, $\dot{m}_\ell$ = 9 kg/s	28
III.9	Slip Ratio Along Generator, $\dot{m}_\ell$ = 9 kg/s	29
III.10	Pressure Along Generator, $\dot{m}_\ell$ = 9 kg/s	30
III.11	Local Load Factor Along Generator, $\dot{m}_\ell$ = 9 kg/s	31
III.12	Void Fraction Along Generator, $\dot{m}_\ell$ = 9 kg/s	32
III.13	Influence of Liquid Flow Rate on Generator Efficiency at B = 0.6T and R_L = 0.4mΩ	33
III.14	Comparison of ANL Generator Efficiencies for $R_L \approx$ 0.25 mΩ	34
III.15	Influence of Liquid Flow Rate on Average Slip Ratio	36
III.16	Slip Ratios Along Generator, χ = 0.01	38
III.17	Pressure Along Generator, χ = 0.01	39
III.18	Void Fraction Along enerator, χ = 0.01	40
III.19	Slip Ratios Along Generator, χ = 0.006	41
III.20	Pressure Along Generator, χ = 0.006	42

LIST OF FIGURES (contd.)

No.	Title	Page
III.21	Void Fraction Along Generator, χ = 0.006	43
III.22	Generator Experiments to Show Liquid-to-Gas Heat Trasnfer, Gas Enters Colder than Liquid	45
III.23	Generator Experiments to Show Liquid-to-Gas Heat Transfer, Liquid Enters Hotter than Gas	46
III.24	Distributions of Magnetic Flux Densities and Pressure Along the Generator	48
IV.1	The Effect of a Solid Particle on a Bubble	50
IV.2	Potential Bubble Coalescence	50

LIST OF TABLES

No.	Title	Page
III.1	Comparison of Generator Data with Old and Revised Loops, $\dot{m}_{\ell}$ = 6 kg/s, Back Pressure = 0.14 MPa Gauge (20 psig)	17
IV.1	Wetting Experiments--NaK on Carbon Steel and Stainless Steel . .	57
IV.2	Contact Angle Measurements in NaK (eutectic) Alloy	60
IV.3	Surface Tension Measurements on NaK 77 Systems at Room Temperature	68

NOMENCLATURE

SYMBOL	DEFINITION
a	Electrode spacing
A	Area
B	Magnetic flux density
c	Bulk concentration of solute
C'_d	Bubble parameter
d	Diameter
D_b	Typical bubble length scale
E	Surface elasticity, Eqs. IV.2 or IV.3
f	Friction factor
F	Load factor, $V_L/u_\ell aB$
Fr	Froude number, Eqs. III.1 and III.2
g	Acceleration of gravity
J	Current density
K	Slip ratio
L	Generator length
$\dot{m}$	Mass flow rate
$\bar{M}$	Hartmann number $\frac{W}{2} B \sqrt{\sigma/\mu}$
M	Modified Hartman number
NI_{exc}	Ampere-turns to produce applied magnetic flux density
P	Pressure
$P_{s.t.}$	Pressure in separator tank
Q	Volumetric flow rate
R	Gas constant

Re	Reynolds number, $\rho ud/\mu$
R_e	Equivalent external resistance
R_i	Internal generator resistance
R_L	Load resistance
T	Absolute temperature
u	Velocity
V_L	Load voltage
V_{oc}	Open-circuit voltage of equivalent circuit
w	Channel height parallel to B
α	Void fraction
γ	Surface tension
Γ_2^1	Gibbs absorption isotherm, Eq. IV.1
η	Generator efficiency
λ	Normalized pressure gradient, $-(\Delta p/\Delta \ell)2d/\rho u^2$
μ	Absolute viscosity
μ_2	Chemical potential of solute
ρ	Density
σ	Electrical conductivity
ϕ	Conductivity ratio
x	Mixture quality, $\dot{m}_g/(\dot{m}_g + \dot{m}_\ell)$

Subscripts

g	Gas
ℓ	Liquid
SP	Single phase
TP	Two phase

DEFINITIONS

NAME	SYMBOL	DEFINITION
Bubble Parameter	C'_d	Empirical 'drag coefficient,' based on experimental data, used to calculate slip force between gas and liquid.
Load Factor	F	Ratio of load (electrode) voltage to induced voltage, $V_L/u_\ell aB$.
Void Fraction	α	Ratio of volume occupied by gas to total volume, or flow cross-sectional area occupied by gas to total cross-sectional area.
Mixture Quality	χ	Ratio of gas mass flow rate to total mass flow rate, $\dot{m}_g/(\dot{m}_g + \dot{m}_\ell)$.
Slip Ratio	K	Ratio of gas to liquid velocity.

SUMMARY

Testing of the second diverging-channel generator with the revised ambient-temperature NaK-N_2 facility has been completed. The primary goal of the revised facility, demonstrating reduced slip ratio (ratio of gas velocity to liquid velocity) with higher liquid velocity (flow rate), was accomplished. The reduction in slip ratio was dramatically demonstrated by a series of consecutive runs with varying flow rate (from 6 kg/s to 12 kg/s for the liquid). Substantial increases in generator efficiency were obtained with higher liquid flow rates.

Experiments to demonstrate that good liquid-to-gas heat transfer exists in the generator were successfully completed. Good heat transfer is essential because it is the almost-constant-temperature expansion of the gas (vapor) in the generator that yields the higher system efficiencies for liquid-metal MHD power cycles.

The feasibility of generating relatively-stable bubbles, hence, a foam, in liquid metals has been demonstrated. Photographic documentation of these phenomena, both motion and still pictures, was made. Surface tension measurements and foaming experiments have shown that viscosity is also a factor in promoting bubble formation and persistence. Wetting and contact angle measurements have been made for stainless steel and carbon steel immersed in eutectic NaK.

An analytical study of the liquid shunt (wall) layer sizes and losses has shown that these losses are not expected to be significant for large generators; less than 1.0% decrease in efficiency is anticipated. A two-phase pressure-gradient correlation developed for MHD flows has been shown to agree to within 20% with the generator data.

I. INTRODUCTION

The two-phase LMMHD (liquid-metal MHD) generator program combines experimental and analytical studies in an effort to understand better the physical processes occurring in two-phase generators and to establish the limits of generator performance. For the past seven years this program has been sponsored by the Power Branch of the Office of Naval Research.

The generator experiments are conducted with an ambient-temperature NaK-N_2 test facility, consisting of a two-phase mixer, MHD generator, magnet, and required auxiliary loop equipment. The original facility, used in all tests through July 1975, has been described elsewhere.[1] The revised facility, completed in 1977, is described in Ref. 6. Earlier experiments on generators with varying geometries have been performed and the results presented in previous annual reports.[2,3,4]

Analytical models of the generator have been developed to aid in the basic understanding of the flow characteristics in the generator and to provide a (one-dimensional) computer code capable of predicting approximately generator performance from the independent input parameters such as flow rate, magnetic field strength, and geometry. This computer code and the semi-empirical technique used in characterizing the bubble parameter (churn-turbulent drag coefficient) used in the determination of the interfacial slip ratio have been reported in detail.[2,5]

The channel contours used in or proposed for generator experiments are compared in Fig. I.1. The first channel (LT-1) was designed for a slip ratio of unity, because the actual slip ratio was not known, but higher

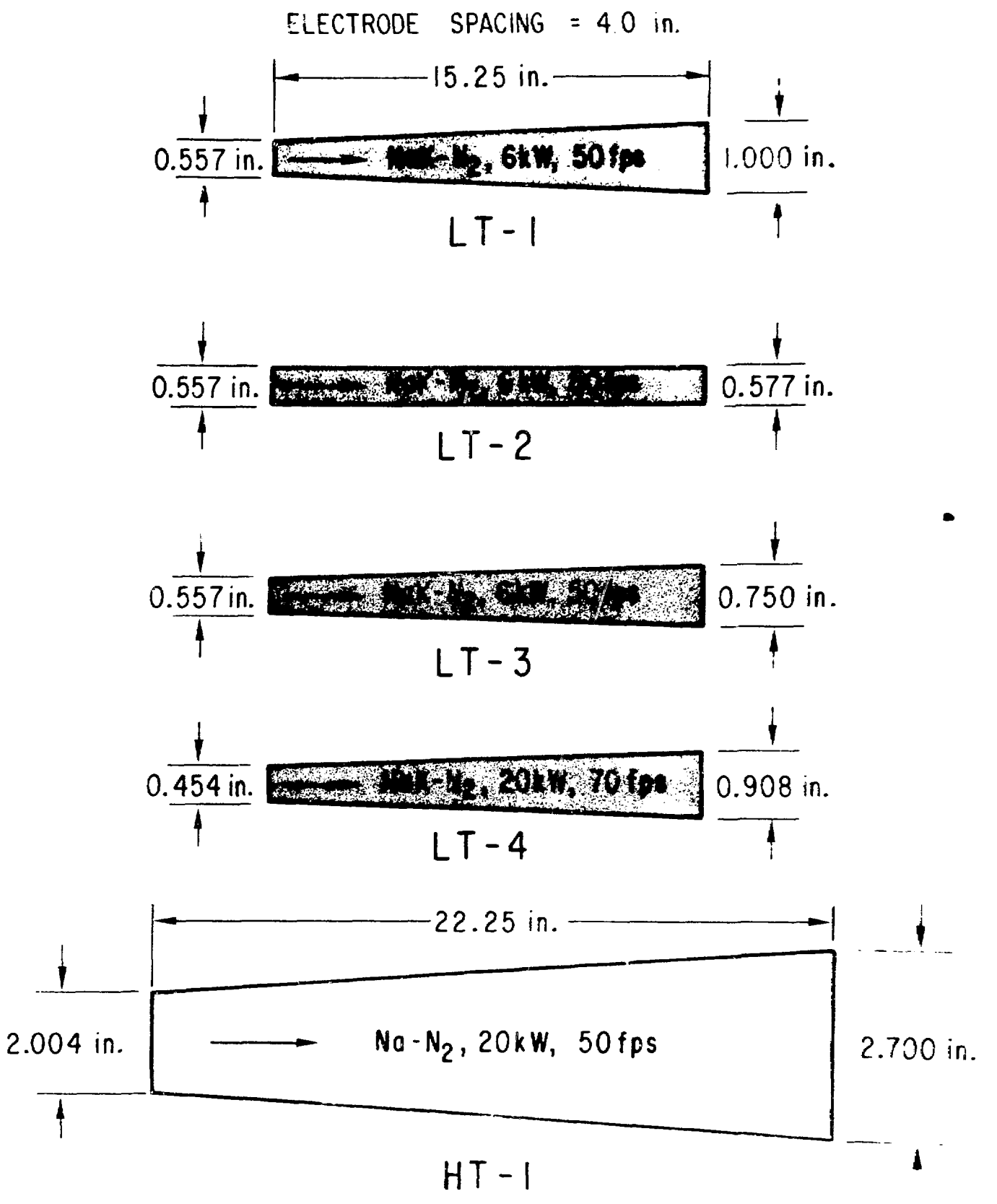

Figure I.1 Channel contours used in ANL LMMHD generator experiments

slip ratios were observed experimentaly and it was noted that the liquid velocity was not constant, it decreased along the generator.[2] A constant-area channel (LT-2) was then tested, and the velocity increased along the channel.[2,3] The second diverging channel (LT-3) has a smaller angle than the first channel, as shown in Fig. I.1, to yield close-to-constant liquid velocity at the design point. As has been described,[4,6] improved generator performance was obtained with LT-3, and the liquid velocity was almost constant. The new high-pressure, high-velocity channel (LT-4) has been designed to utilize the full NaK-nitrogen loop pressure and flow-rate capabilities, and fabrication is almost completed. The first channel for testing in the high-temperature sodium-nitrogen test facility (HT-1) is being fabricated and will be tested at temperatures to 810 K, flow rates to 0.035 m^3/s sodium, and pressures to 700 kPa.

The program, described in Section II, consists of further NaK-N_2 tests on the LT-3 channel, the foam experiments, and the analytical studies. The results of the generator tests, presented in detail in Section III, include comparative data on runs using the same generator with the original and with the revised facilities, and on the influence of higher flow rates on generator performance, and experiments on liquid to gas heat transfer. The foams and surface-active agents experiments, described in Section IV, indicate that good foams can be generated with NaK. The conclusions and suggestions for future work are given in Section V.

II. PROGRAM

II.1 NaK-N_2 Generator Experiments

The NaK-nitrogen flow facility used for the generator tests is shown in Fig. II.1, and the channel used in Fig. I.1. The significant parameters for all of the experimental runs from October 1976 through September 1977 are summarized in Appendix A, and the data is discussed in Section III. The points covered include the repeated generator runs under the same operating conditions, the influence of flow rate on generator efficiency and slip ratio, and the experimental demonstration of good liquid-to-gas heat transfer in the generator.

II.2 Foams

The slip loss caused by the difference in the phase velocities is one of the major loss mechanisms in two-phase liquid-metal MHD generators, especially at the high void fractions required for efficient cycle operation. One way to reduce this loss is to produce a more-stable foam flow by means of surface-active agents. The potential gains in generator and cycle performances make this approach very attractive. Thus, a program to evaluate surface-active agents was initiated, and the results from the first full year of study are reported in Section IV.

Foams and surface-active agents are treated extensively in the literature, but there is virtually no information on liquid-metal foams. However, the available literature on the characterization of aqueous and organic foams provides some insight into the preparation of a liquid-metal foam. This literature contains frequent references to the use of

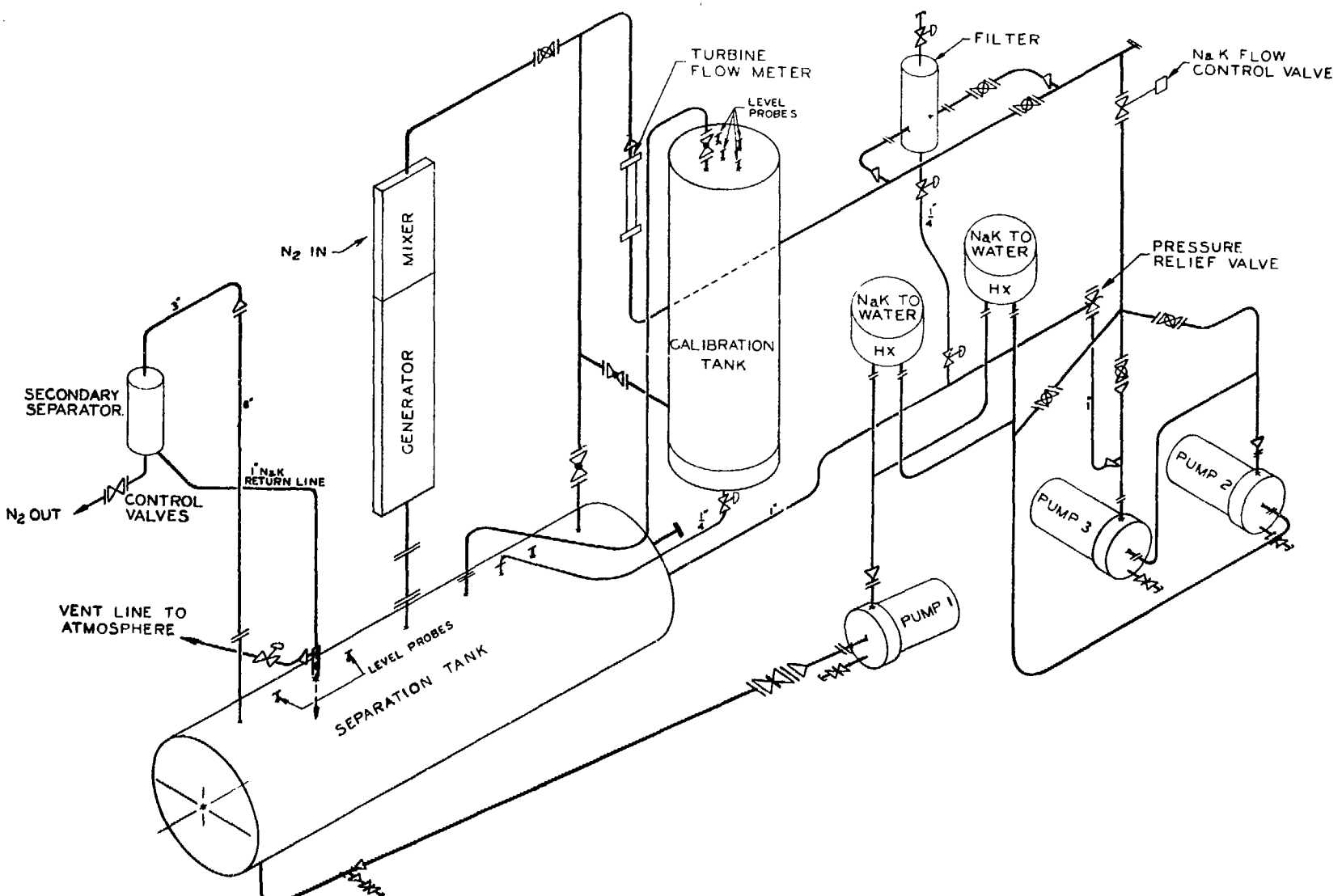

Figure II.1. NaK-Nitrogen Flow Loop

surface-active additives, and surface tension and viscosity appear to be the most relevant physical properties of interest. Therefore, studies have been initiated which focus on the effect of surface-active agents as liquid-metal foam promoters and on the potential for fine particle suspensions to act as foam stabilizers. Viscosity and surface tension were selected as the first physical properties to be measured and evaluated for use in the correlation of systems of differing bubble behavior.

NaK was chosen for these initial experiments because it allows room-temperature tests without the special problems associated with handling hot liquid metals. Thus, the concept of using surface-active agents in MHD generators can be evaluated more rapidly and inexpensively with NaK, the existing NaK facility is available for future flow tests, and a generator of known performance properties with pure NaK will be available to observe the changes with a foam.

The use of both particulate dispersions and soluble additives to NaK to produce foams is discussed in Section IV, as is the experimental approach used to observe NaK foamability. The wetting aspects, surface tension, viscosity, and bubble performance data are summarized in the same Section.

II.3 Analytical Studies

II.3.1 Shunt Layer*

It is not possible in a two-phase LMMHD generator to avoid the presence of a liquid shunt layer on the insulating (or non-electrode) duct walls. Practical experience has shown that, indeed, such a layer forms, and experiments to eliminate it have been conducted.[4] In the current study, a different approach is taken, i.e., the determination of the magnitude of the shunt

* Supported in part by the U.S. Department of Energy

layer influence on generator performance as a function of generator size. This study results are summarized here, and presented in detail in Ref. 7.

The flow in the rectangular two-dimensional duct is assumed to consist of a homogeneous two-phase core (Region 1), with the walls wetted by a pure liquid layer (Region 2). The equations are solved by using the standard Hartmann layer approximation. As long as the shunt (liquid) layer thickness is larger* than the Hartmann layer thickness $\simeq 1/M_2$, the generator efficiency, η, depends on the load factor F and modified Hartmann number $\bar{M}$ as

$$\eta = \frac{F(1 - F)\bar{M}}{[(1 - F)\bar{M} + F]}, \qquad \text{(II.1)}$$

where

$$\bar{M} = M_1 \sqrt{\left(\frac{\mu_1}{\mu_2}\right)\left(\frac{\sigma_1}{\sigma_2}\right)}, \qquad \text{(II.2)}$$

$$M_1 = \frac{w}{2} B \sqrt{\sigma_1/\mu_1}, \qquad \text{(II.3)}$$

B is the magnetic flux density, w is the channel height parallel to B, μ and σ are the fluid absolute viscosity and conductivity, and the subscripts 1 and 2 refer to the two-phase core and shunt layer regions respectively. The load factor is defined as

$$F \equiv \frac{R_e}{R_i + R_e}, \qquad \text{(II.4)}$$

* If the shunt (liquid) layer thickness is larger than the Hartmann layer thickness, the electrical conductivity and, hence, the shunt-layer current will be reduced, and the decrease in generator efficiency will be less than calculated here.

where R_i is the internal resistance of the generator and R_e is the equivalent external resistance. Equation II.1 includes ohmic, friction, and shunt losses, and assumes that all of the external current flows through the load resistance. It can be modified to include the effects of end currents, wall currents, etc.

The comparable expression to Eq. II.1 for an homogeneous Hartmann flow is

$$\eta = \frac{F(1 - F)(M - \tanh M)}{[(1 - F)M + F \tanh M]} , \qquad \text{(II.5)}$$

which becomes Eq. II.1 with $\bar{M}$ replaced by M for large M, so that $\tanh M \to 1$ and $(M - \tanh M) \to M$.

The efficiency can be rewritten as

$$\eta = \frac{F}{\left[1 + \frac{F}{(1 - F)\bar{M}}\right.} \qquad \text{(II.1a)}$$

and this expression makes it clear that for large $\bar{M}$ the effect of the shunt layer on η is small. For $F = 0.9$ and $\bar{M} = 1000$, the second term in the denominator is 0.009 and η is reduced from 0.9 to 0.892. If $\bar{M} = 2000$, than η is 0.896. The efficiency, Eq. II.1, is shown in Fig. II.2 as a function of F and $\bar{M}$.

In large LMMHD generators, values of M_1 on the order of 5000 are anticipated. Because μ_1/μ_2 increases with increasing void fraction, whereas σ_1/σ_2 decreases, $\bar{M}$ is estimated to be at least half of M_1 and the shunt layer losses are negligible. Thus, shunt losses are not expected to be significant for large generators, provided an homogeneous core flow is established.

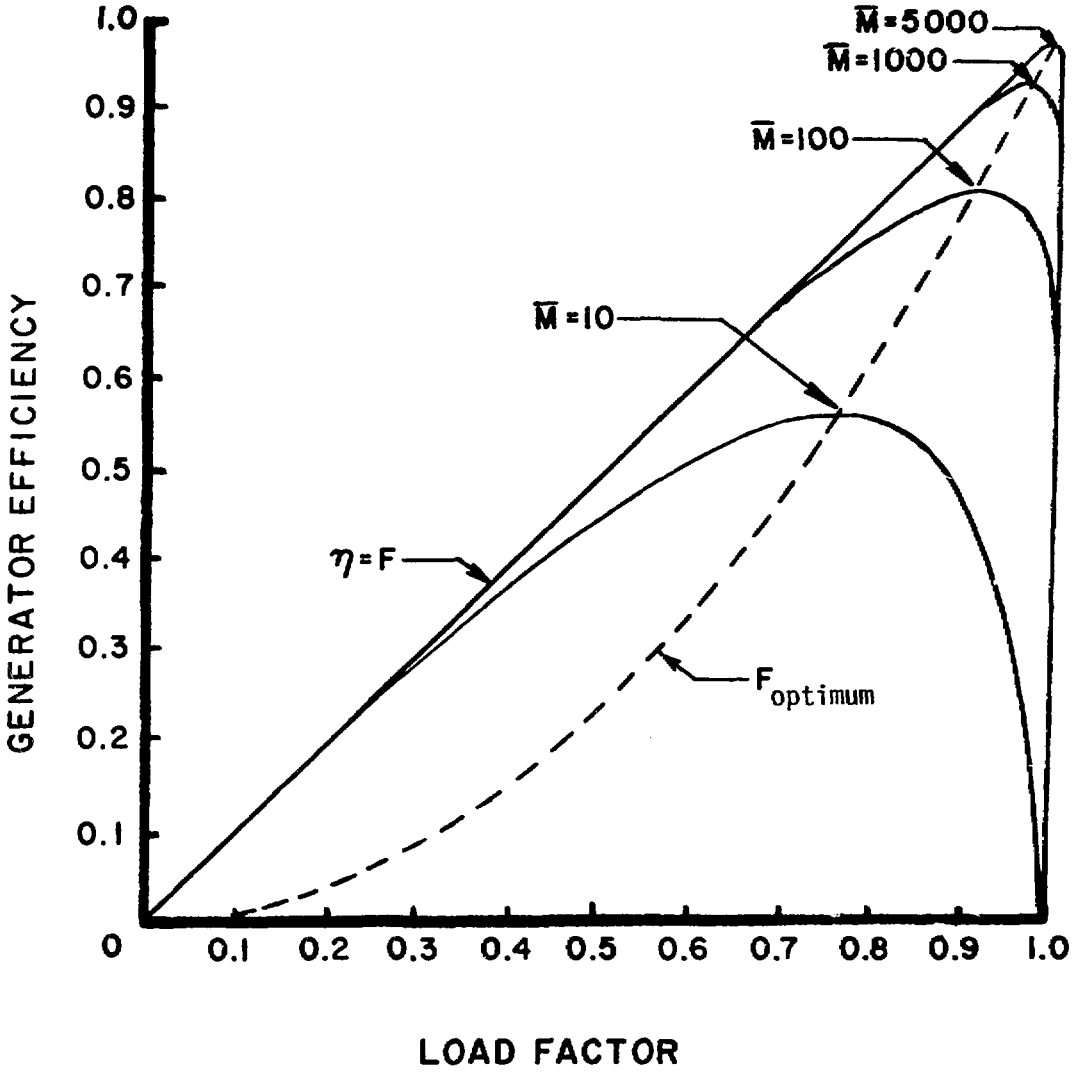

Figure II.2 Generator Efficiency vs. Load Factor for Various Hartmann Numbers

II.3.2 Pressure-Gradient Correlation

The theoretical single-phase (pure liquid) normalized pressure gradient for MHD pipe flow is[8]

$$\lambda^*_{sp} = \frac{2M_{SP}}{Re_{SP}} \frac{(M_{SP}\phi'_{SP} + 1)}{(\phi'_{SP} + 1)}, \qquad (II.6)$$

where the subscript SP denotes pure liquid and the single-phase normalized resistance coefficient is defined as

$$\lambda^*_{SP} \equiv \lambda_{SP,M} - \lambda_{SP,M=0}$$

$$= \left[\left(-\frac{\Delta p}{\Delta \ell}\right)_M - \left(\frac{\Delta p}{\Delta \ell}\right)_{M=0}\right] \frac{2d}{\rho u^2}. \qquad (II.7)$$

The Hartman and Reynolds numbers are

$$M_{SP} \equiv Bd\sqrt{\sigma/\mu} \qquad (II.8)$$

and

$$Re_{SP} \equiv \rho ud/\mu, \qquad (II.9)$$

and the conductivity ratio is

$$\phi'_{SP} \equiv 2w(\sigma_w + 1/R_c)/\sigma d. \qquad (II.10)$$

Here d is the equivalent pipe diameter, u the average mean velocity, $\Delta p/\Delta \ell$ the pressure difference over a length ℓ (normally the magnet pole face length), w and σ_w the pipe wall thickness and electrical conductivity, R_c the contact resistance between the liquid and pipe wall, and ρ, σ, and μ the liquid density, electrical conductivity, and absolute viscosity.

Equation II.6 can be extended to cover two-phase flow (denoted by the subscript TP) by defining the two-phase velocity and electrical conductivity as

$$u_{TP} = u_{SP}/(1 - \bar{\alpha}) \qquad (II.11)$$

and

$$\sigma_{TP} = \sigma_{SP} \exp(-3.8\bar{\alpha}), \qquad (II.12)$$

where $\bar{\alpha}$ denotes the average void fraction. (Equivalent two-phase expressions for density and absolute viscosity as a function of $\bar{\alpha}$ were also used initially; however, the data were predicted well without the use of these two equivalent expressions). These two-phase expressions yield

$$M_{TP} = M_{SP} \exp(-1.9\bar{\alpha}), \qquad (II.13)$$

$$Re_{TP} = Re_{SP}/(1 - \bar{\alpha}), \qquad (II.14)$$

and

$$\phi'_{TP} = \phi'_{SP} \exp(3.8\bar{\alpha}). \qquad (II.15)$$

The expression for the two-phase normalized resistance coefficient analogous to Eq. II.6 is[7,9]

$$\lambda^*_{TP} = \frac{2M_{SP}}{Re_{SP}} \left[\frac{M_{SP}\,\phi'_{SP} \exp(1.9\alpha) + 1}{\phi'_{SP} \exp(3.8\alpha) + 1} \right] (1 - \alpha) \exp(-1.9\alpha) \qquad (II.16).$$

This equation can alternatively be derived along the lines of Lockhart and Martinelli.[10]

The two-phase correlation, Eq. II.16, is compared in Fig. II.3 with some of the generator experimental data. (The analytical expressions for the normalized resistance coefficient for a loaded LMMHD generator and for a conducting-wall circular pipe are similar when $M_{SP}\,\phi'_{SP} \gg 1$.) In the correlation, $\phi'_{SP} = (1 - \bar{F}_{SP})/\bar{F}_{SP}$, is used, where $\bar{F}_{SP}$ is the average load factor ($\equiv V_T/uBh$) for pure liquid. The agreement is good, to within 20%.

II.3.3 Imperfect Compensation

Unless compensation is provided for the induced magnetic field caused by the currents in the conducting fluid, the total magnetic field

	DATE	$\dot{m}_\ell$ (Kg/S)	R_L ($\mu\Omega$)	B (T)
△	2-18-77	5.98	400	0.59
x	2-25-77	6.00	250	0.59
o	3-04-77	3.01	250	1.20
+	3-07-77	6.00	250	1.20

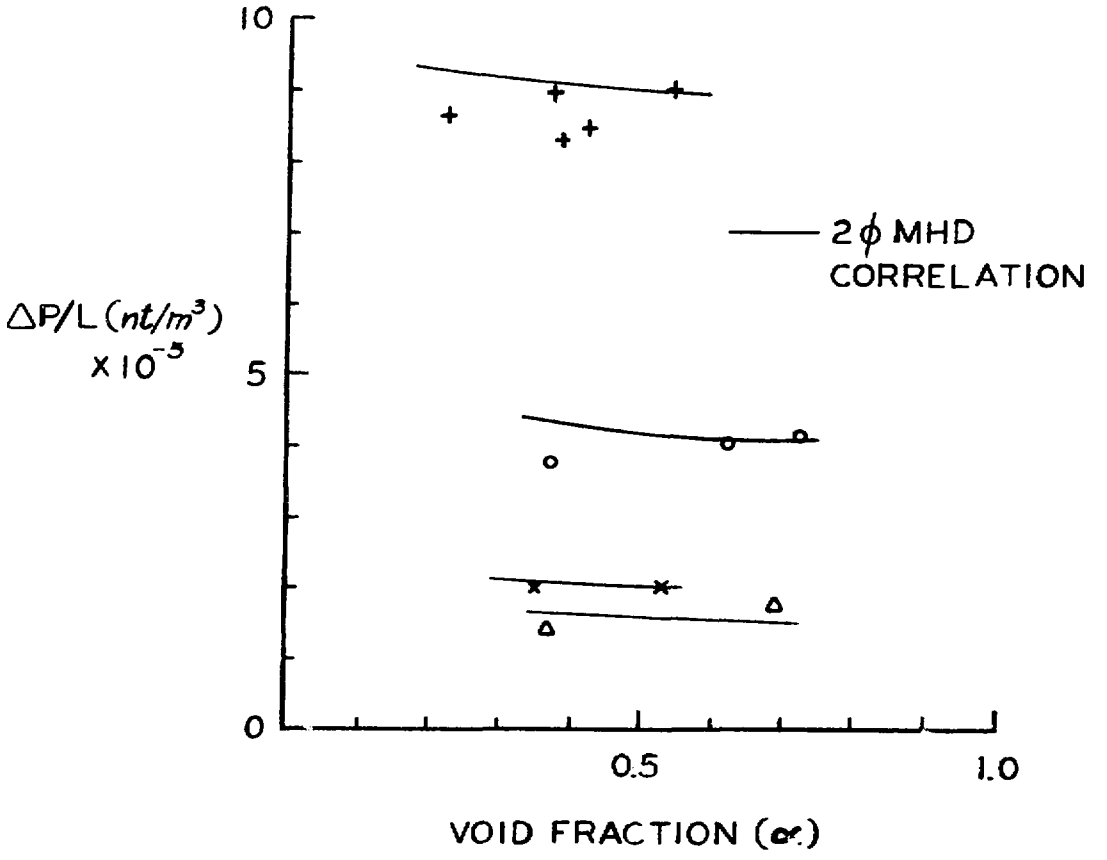

Figure II.3 Comparison of Two-Phase MHD Pressure-Gradient Correlation with Ambient-Temperature NaK-N_2 Generator Data

varies exponentially along the channel and, for a generator, most of the energy conversion occurs in the downstream end of the channel. The result is a reduced generator efficiency. (A similar phenomenon, called armature reaction, occurs in dc rotating machines.) To eliminate the induced field or compensate the generator, the fluid current is returned through the air gap of the electromagnet. If the compensation is perfect, i.e., the return current is at the same axial location as the fluid current, the induced field lies along the flow and has no effect on the generator. However, because of both end currents and varying fluid properties and velocity along the flow the compensation will be imperfect, as shown by experiments.[4,11] The objective of this analytical study is to model the distortion caused in the magnetic field by imperfect compensation, and to assess the consequent effect on generator performance.

A one-dimensional model has been developed to indicate general trends with minimum computer time, where all of the vector quantities have only one component and all variables depend only on the axial location along the channel. Following a procedure similar to Bertinov and But,[12] a Fredholm integral equation for the induced magnetic field, given the distribution of MHD channel and compensation currents, has been derived for ideal iron. A PL/1 code has been written and debugged to solve for the total magnetic field as the sum of the applied and induced fields. In the code, the electrode voltage is assumed, the compensation current distribution determined by using a current divider and the specified load resistance, and the channel current is calculated. The load current is then varied until it matches the channel current.

A two-dimensional model is also being developed to give a more-accurate solution, where all vector quantities have one component except for the magnetic field, which has two components, and all variables can depend

on both the axial location along the channel and the location along the axis parallel to the applied magnetic field. The total magnetic field is determined by TRIM, a Fortran magnet design code that uses an irregular triangular mesh, finite-element method to solve for the magnetic vector potential, given the geometry, the distribution of currents, and the material magnetic properties.[13] (The version used here has been slightly modified from that obtained from the Accelerator Research Facility at ANL.) A PL/1 code determines the MHD channel and compensation currents for a specified magnetic field, and these currents are then used in TRIM to determine a new magnetic field. The PL/1 code and TRIM are used sequentially until the magnetic field converges to a solution. These two codes have been run separately and are now ready to be run in sequence.

III. GENERATOR PERFORMANCE

Repeat runs of some of the previous cases were made, and the old and new results are compared in Section III.1. The influence of higher flow rates or velocities on generator efficiency and slip ratio is shown in Section III.2. The experimental demonstration of good liquid-to-gas heat transfer is described in Section III.3, and the effect of magnetic field shaping by tapered iron pole faces in Section III.4. A summary of all of the experimental data for the period from October 1976 to September 1977 is given in Appendix A.

III.1 Comparison with Previous Data

Sets of data with the old loop (7/7/75), the revised loop immediately after construction (8/18/76 and 8/24/76), and the revised loop recently (2/7/77) are listed in Table III.1. (The first three sets were previously reported in Ref. 6.) The efficiency as a function of quality was virtually unchanged, with the exception of the zero-quality runs (see below). However, as shown by the data for a quality of about 0.0058, the power level (pressure difference and voltage) was substantially higher (about 35% after correction for unequal magnetic fields) for the runs immediately after construction as compared to the runs with the old loop. The difference has decreased for the recent runs, but the power level is still higher than with the old loop.

The runs with the highest power level (August 1976) had a lower measured average velocity slip ratio K (ratio of gas to liquid velocity), implying that a more-uniform two-phase mixture existed in the generator, the liquid velocity was higher (higher voltage, current, and pressure drop), and the exit void fraction (ratio of gas volume to

Table III.1

Comparison of Generator Data with Old and Revised Loops, $\dot{m}_\ell$ = 6 kg/s, Back Pressure = 0.14 MPa Gauge (20 psig)

Date	x	η_g [%]	B [T]	R_L [mΩ]	V_L [V]	Δp [0.1 MPa]	$\bar{\alpha}$	$\bar{K}$	$\bar{F}$
7/7/75 (old)	0	52.9	1.175	0.255	0.506	2.67	0	-	1.02
	0.00580	49.9	1.16	0.254	0.741	2.62	0.49	1.34	0.76
	0.00979	42.1	1.165	0.258	0.819	2.66	0.64	1.217	0.61
8/18/76 (revised)	0	39.4	1.253	0.26	0.470	3.01	0	-	0.89
	0.00216	48.1	1.24	0.27	0.665	3.31	0.27	1.272	0.93
	0.00567	50.3	1.235	0.27	0.867	3.75	0.49	1.047	0.82
	0.00852	46.4	1.238	0.27	0.932	3.90	0.59	1.007	0.74
	0.0110	43.1	1.235	0.27	1.01	4.16	0.68	0.876	0.62
8/24/76 (revised)	0	42.9	1.223	0.24	0.466	2.98	0	-	0.91
	0.00580	49.2	1.227	0.247	0.824	3.69	0.48	1.180	0.83
	0.00825	44.7	1.227	0.248	0.885	3.90	0.55	1.187	0.77
	0.01118	40.6	1.222	0.247	0.937	4.00	0.62	1.18	0.69
	0.0128	43.8	1.225	0.246	1.003	3.99	0.54	1.74	0.89
2/17/77 (revised)	0	46.4	1.212	0.270	0.471	2.66	0	--	0.92
	0.00229	53.8	1.220	0.272	0.648	2.76	0.25	1.65	0.95
	0.00550	51.6	1.205	0.270	0.818	2.95	0.44	1.54	0.89
	0.00815	48.1	1.205	0.270	0.865	2.84	0.53	1.49	0.81
	0.01108	41.8	1.212	0.269	0.933	3.03	0.60	1.52	0.73
	0.01455	36.3	1.200	0.272	0.992	3.19	0.67	1.51	0.66

total volume) was larger. Also the fluctuation in the generator terminal voltage was reduced, amounting to only a few percent of the average voltage. (Compare this with the previous runs.[4])

The liquid velocities along the generator calculated from the measured void fractions and flow rates for the four runs at about 0.0058 quality are compared in Fig. III.1. Note that the differences in either the variations of or the average liquid velocities are not sufficient to account for the performance differences (except for 2/7/77 where the liquid velocity is definitely lower). An important difference is in the average load factor $\overline{F}$, Table III.1. This is higher for the runs with the revised facility, indicating a higher "effective" liquid velocity-electrical conductivity combination for the new runs. This result is expected from the reduced fluctuations.

It is suspected that the improvement in generator performance for the initial tests with the revised loop, followed by its decay, was due to changes in the surface properties of the NaK. Putting the NaK into the revised loop probably caused a considerable increase in the impurities in the NaK, primarily iron oxide and iron powder from the carbon steel. These impurities could have caused some surface activity in the NaK, and thus increased the stability of the two-phase mixture and decreased the size of the gas bubbles produced by the mixer. Between the two sets of runs with the revised loop (August 1976 and February 1977) the NaK was extensively filtered, and some physico-chemical changes may have occurred.

The zero-quality runs require special comment because the reasons proposed above should have no effect. Comparing the July 1975 and August 1976 runs, the terminal voltage and efficiency were higher for the former

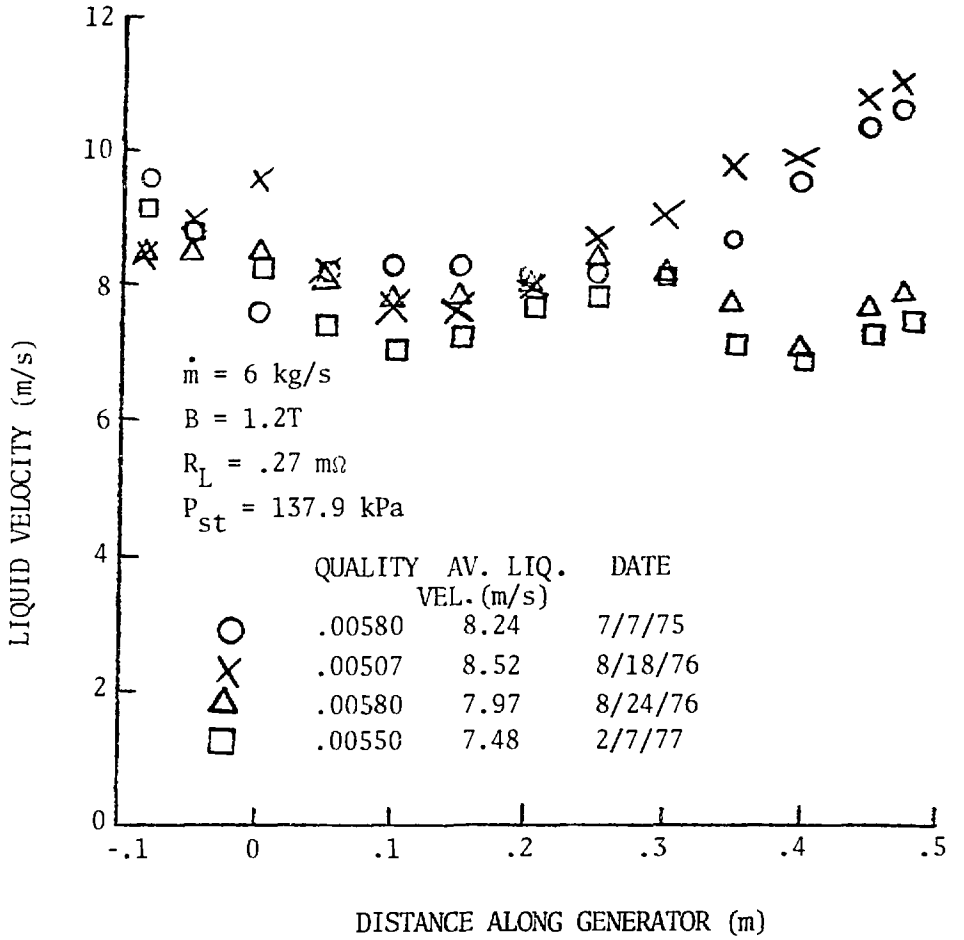

Fig. III.1 Liquid Velocity Along Generator

and the pressure drop was lower. The measured void fraction profiles indicate that flow separation occurred in at least some of the old zero-quality runs, including the August 1976 case. Comparing expected behaviors with and without flow separation, for the latter the liquid velocity should be less at the exit end of the generator, the circulating currents should be higher, and thus the pressure gradient in the upstream part of the generator should be higher. (In the pure liquid case the liquid velocity decreases due to the diverging channel, so that the liquid is pumped in the downstream part of the generator.) This predicted behavior difference is consistent with the data. The suspected higher surface activity could result in improved wetting, and thus less or no flow separation. The February 1977 data fits between the other cases, and this is consistent with the intermediate behavior with gas and proposed intermediate surface activity.

The calculated performance from the generator prediction code is a terminal voltage of 0.477 V and an efficiency of 0.425 at 1.2 T, 6.0 kg/s pure NaK, and 0.25 mΩ load resistance. The August 1976 runs yielded values close to the calculated values.

III.2 Influence of Flow Rate

III.2.1 Efficiency

The effect of increasing the liquid flow rate from 6 kg/s to 9 kg/s is shown in Fig. III.2 for 1.2 T. A load resistance of 0.4 mΩ, rather than the 0.25 mΩ used in most previous runs, reduced the pressure drop and gave a higher efficiency. Higher liquid flow rates or qualities were not used because of the existing mixer's pressure limit. The efficiency increase from 6 to 9 kg/s exceeds ten percentage points at the higher void fractions.

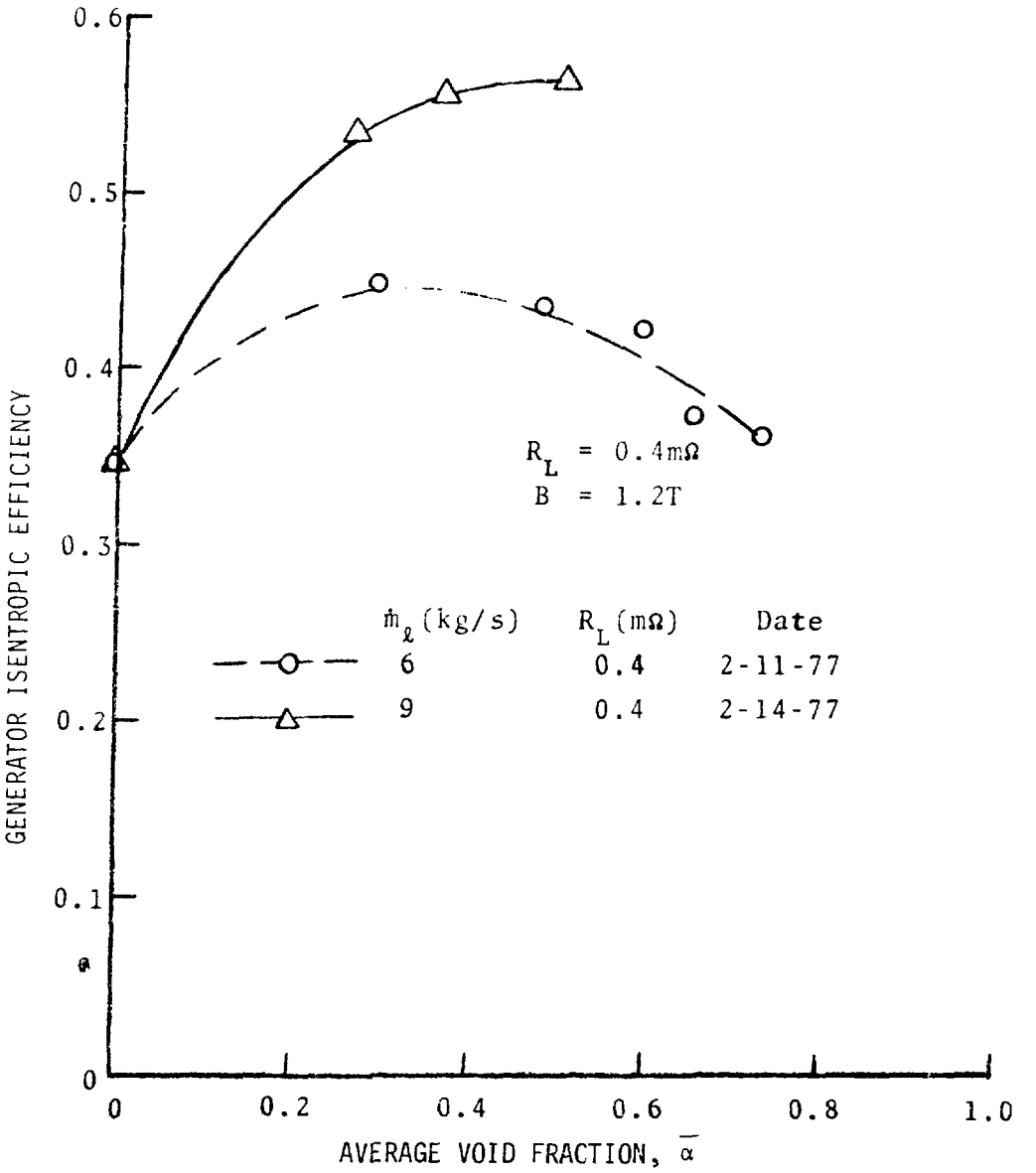

Figure III.7 Influence of Flow Rate on Generator Efficiency, B = 1.2 Tesla.

The liquid velocity, slip ratio, pressure, load factor, and void fraction variations along the generator are shown in Figs. III.3 to III.7 for 6 kg/s, and Figs. III.8 to III.12 for 9 kg/s. The significant differences are: 1) A much larger variation in the liquid velocity along the channel at 9 kg/s since the pressure difference or gradient is higher than the channel was designed for, and 2) A generally lower slip ratio at 9 kg/s. In spite of the increased velocity variation, the efficiency is higher at 9 kg/s because of the reduced slip and slip loss.

The generator efficiencies for 6, 9, and 12 (10.5 for the two highest α values) kg/s at 0.4 m_Ω and 0.6 T (reduced mixer pressure) are shown in Fig. III.13. Again the efficiency increases with liquid flow rate at the higher void fractions.

To compare the higher-flow-rate efficiencies with previously-published results, data for 0.25 m_Ω is shown in Fig. III.14. The curve for 1.2 T, 7/7/75, represents the best performance obtained with the old facility and this load resistance. (Note that the zero quality efficiency is too high for this case due to flow separation, Section III.1.) The three curves for 0.6 T again show the better efficiency at higher liquid velocity. Note that even though the reduced magnetic field would normally be expected to result in lower efficiency, the higher velocity more than compensates.

III.2.2 Slip Ratio

For MHD two-phase flows the slip ratio decreases with increasing Froude number

$$Fr = \frac{\rho_\ell u^2}{\rho g D_b}, \qquad \text{(III.1)}$$

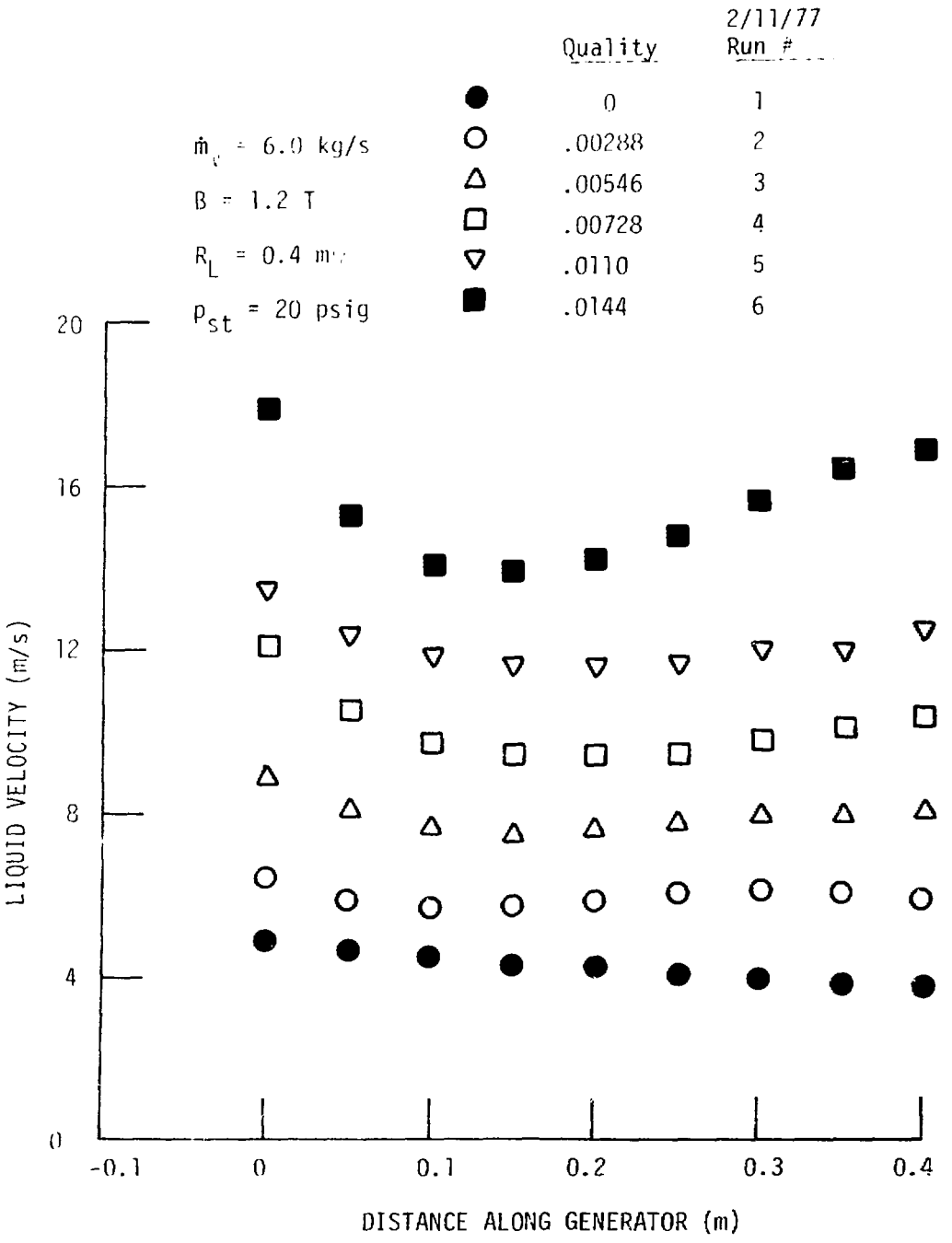

Figure III.3 Liquid Velocity Along Generator, $\dot{m}_\ell$ = 6 kg/s

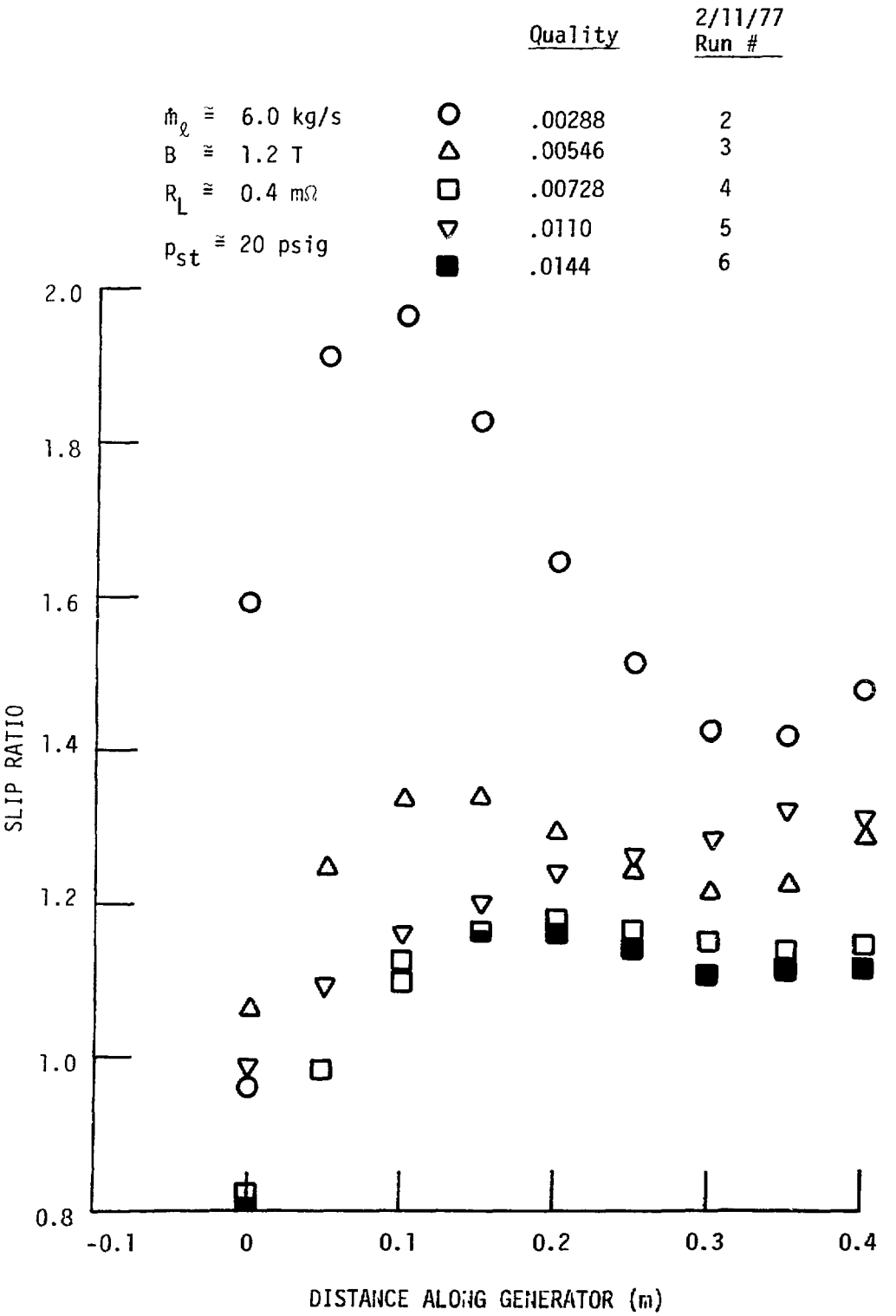

Figure III.4 Slip Ratio Along Generator, $\dot{m}_\ell$ = 6 kg/s

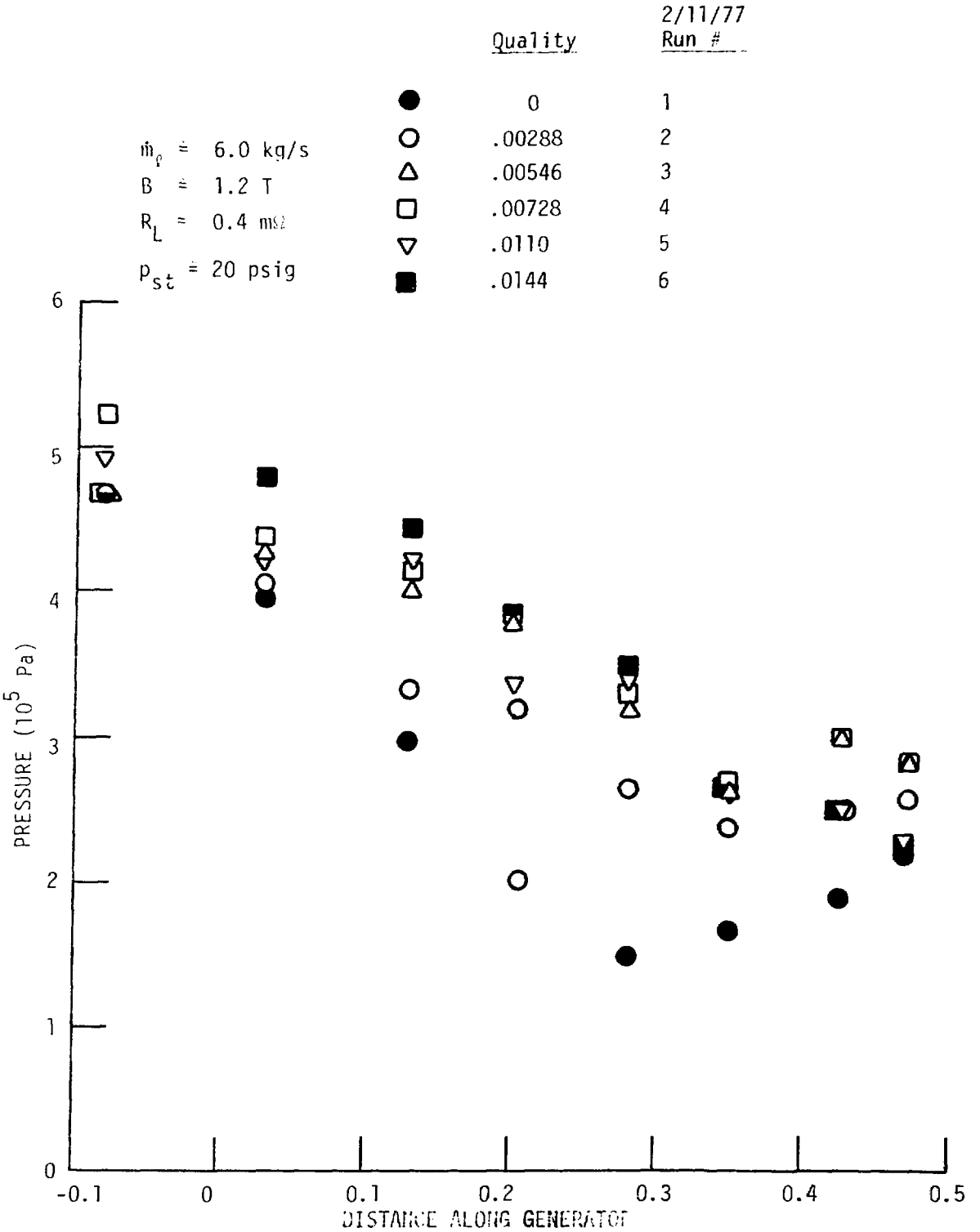

Fig. III.5 Pressure Along Generator, $\dot{m}_\ell$ = 6 kg/s

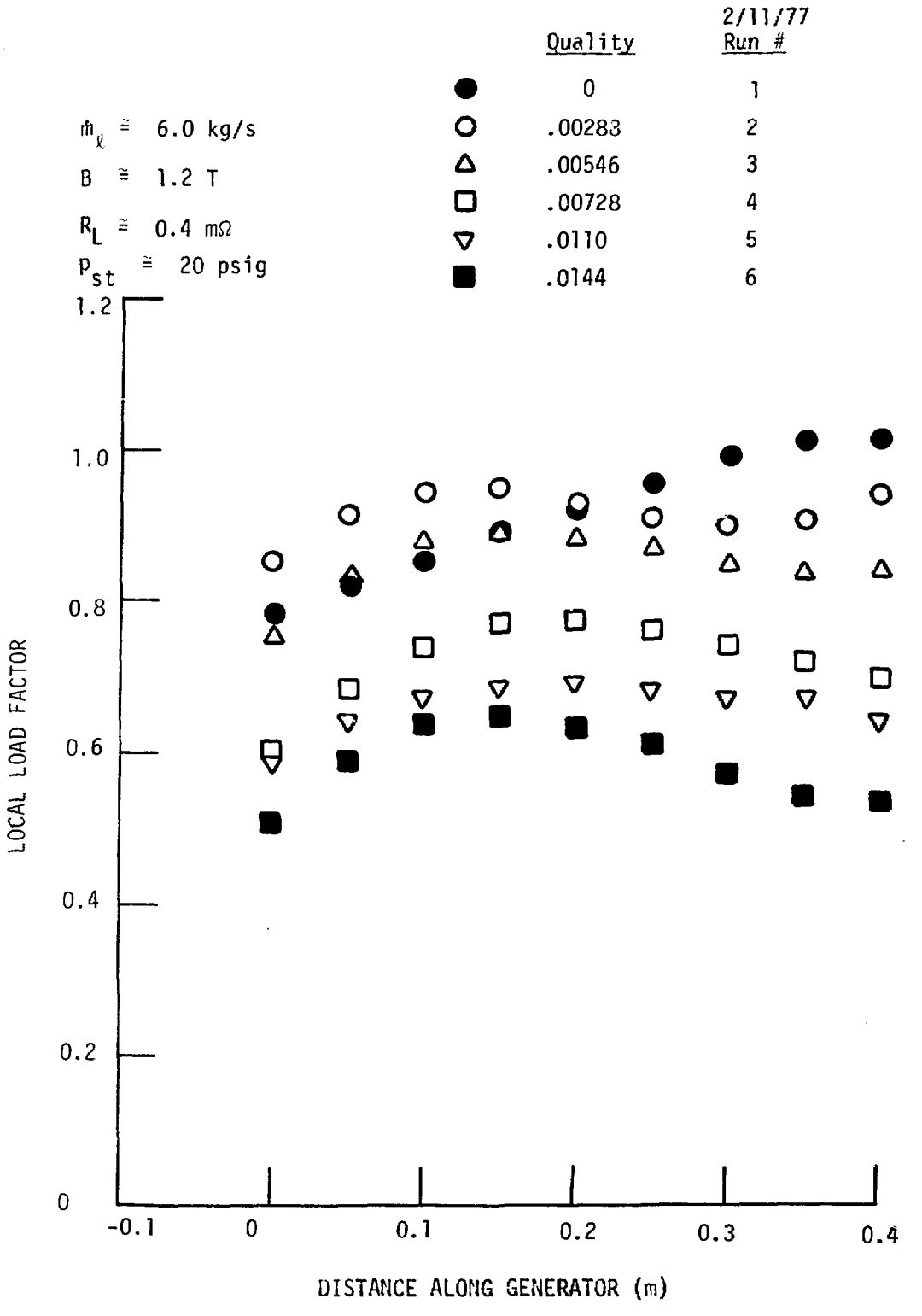

Fig. III.6 Local Load Factor Along Generator, $\dot{m}_\ell$ = 6 kg/s

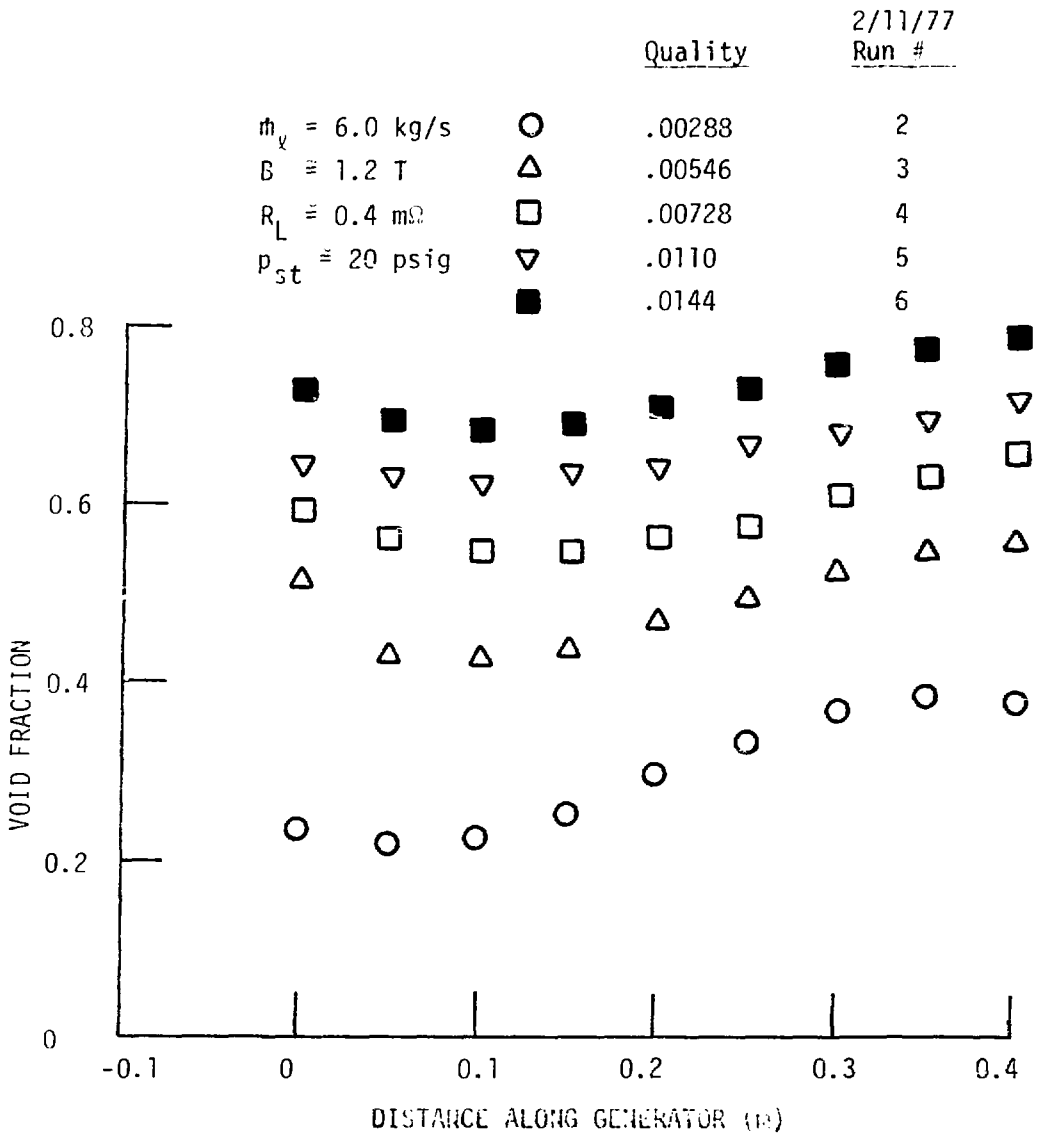

Figure III.7 Void Fraction Along Generator, $\dot{m}_\ell$ = 6 kg/s

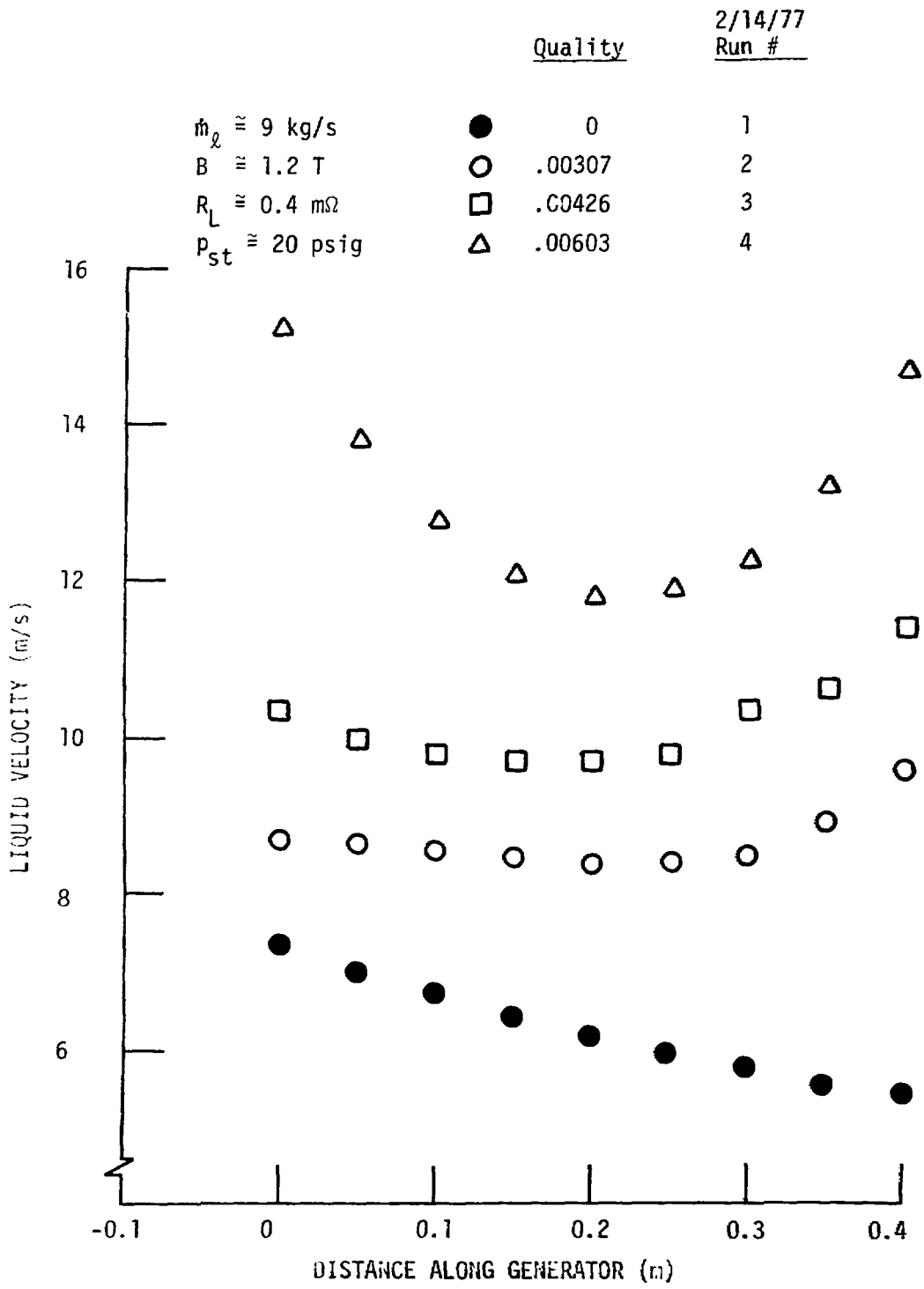

Figure III.8 Liquid Velocity Along Generator, $\dot{m}_\ell$ = 9 kg/s

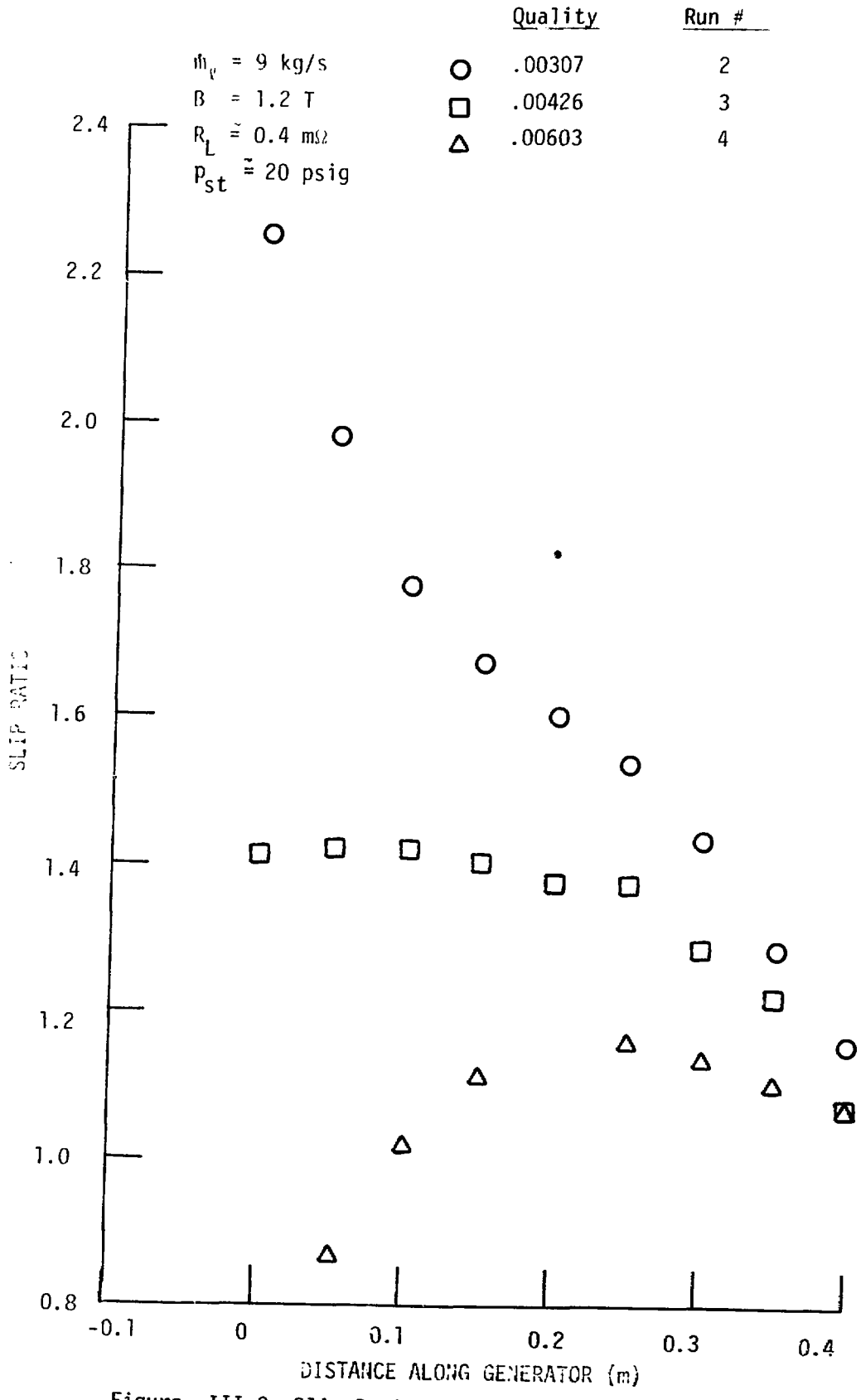

Figure III.9 Slip Ratio Along Generator, $\dot{m}_\ell$ = 9 kg/s

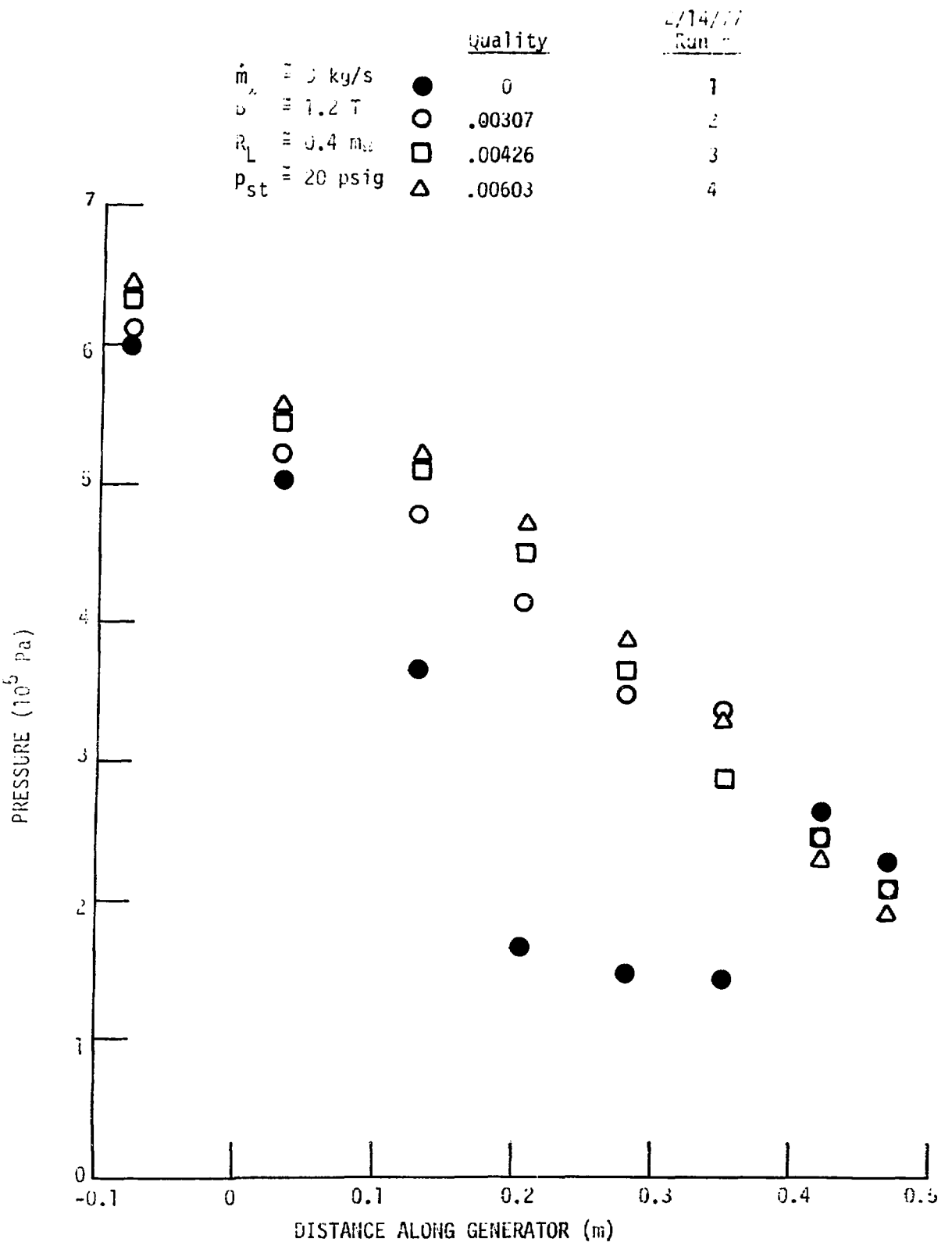

Figure III.10 Pressure Along Generator, $\dot{m}_x$ = 9 kg/s

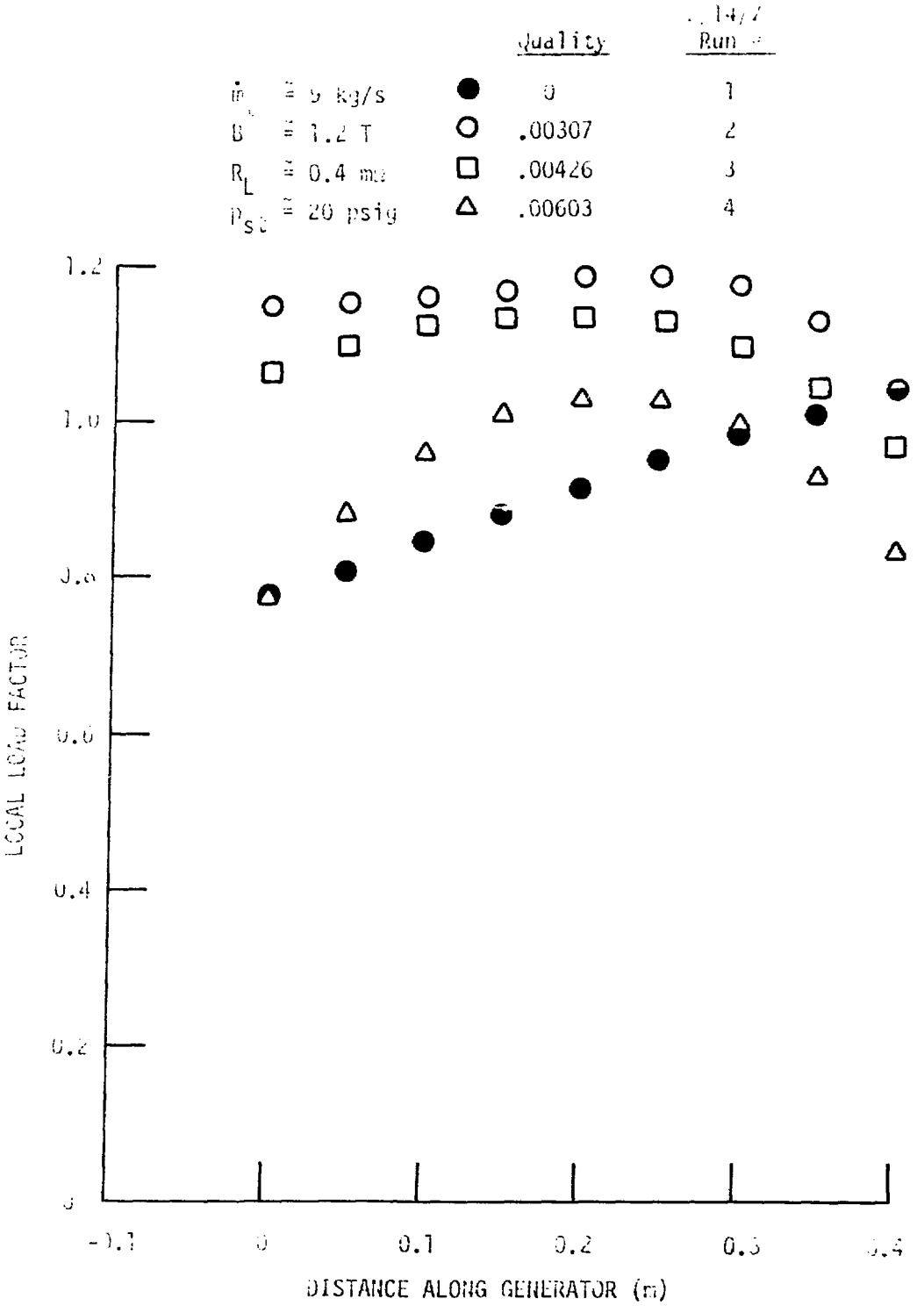

Figure III.11 Local Load Factor Along Generator, $\dot{m}$ = 9 kg/s

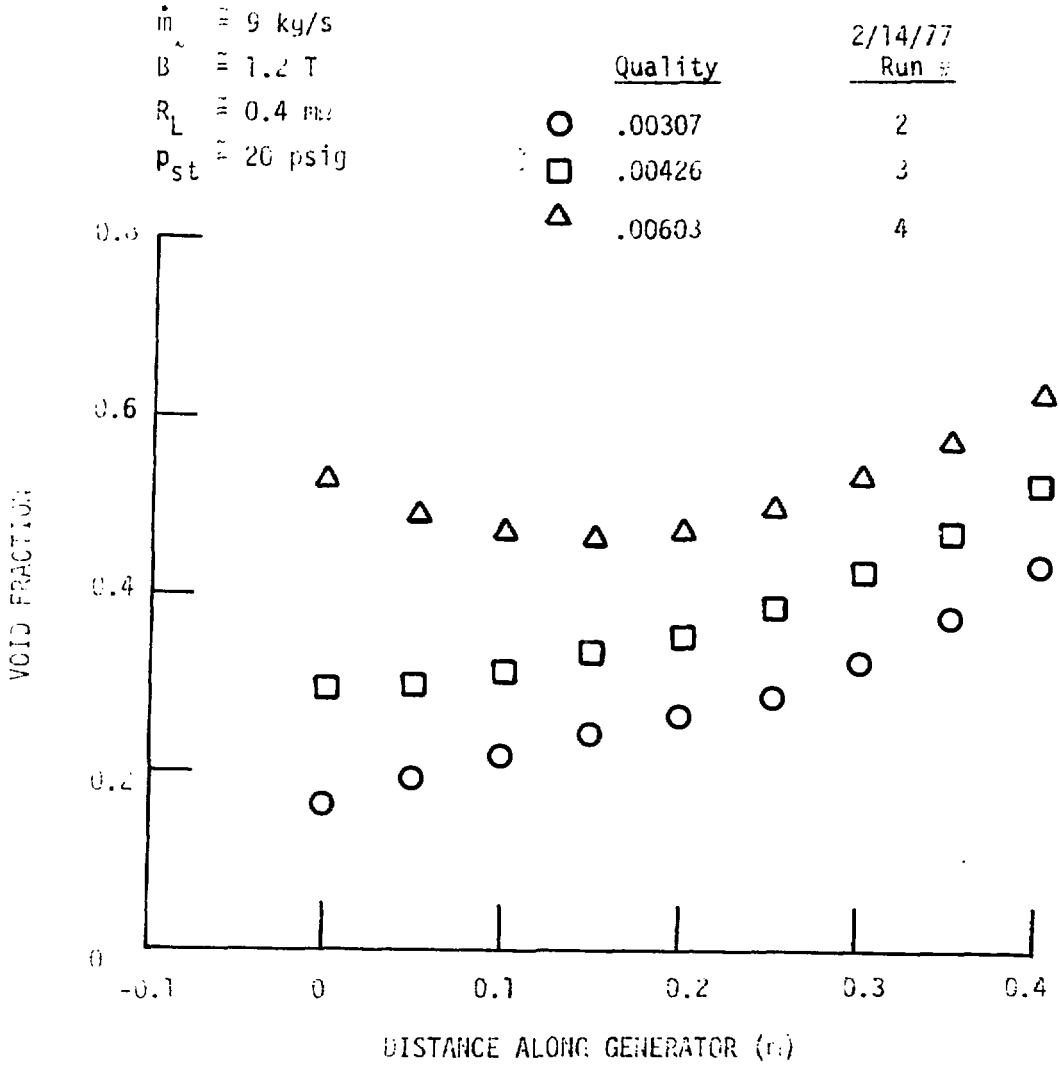

Figure III.12 Void Fraction Along Generator, $\dot{m}_\ell$ = 9 kg/s

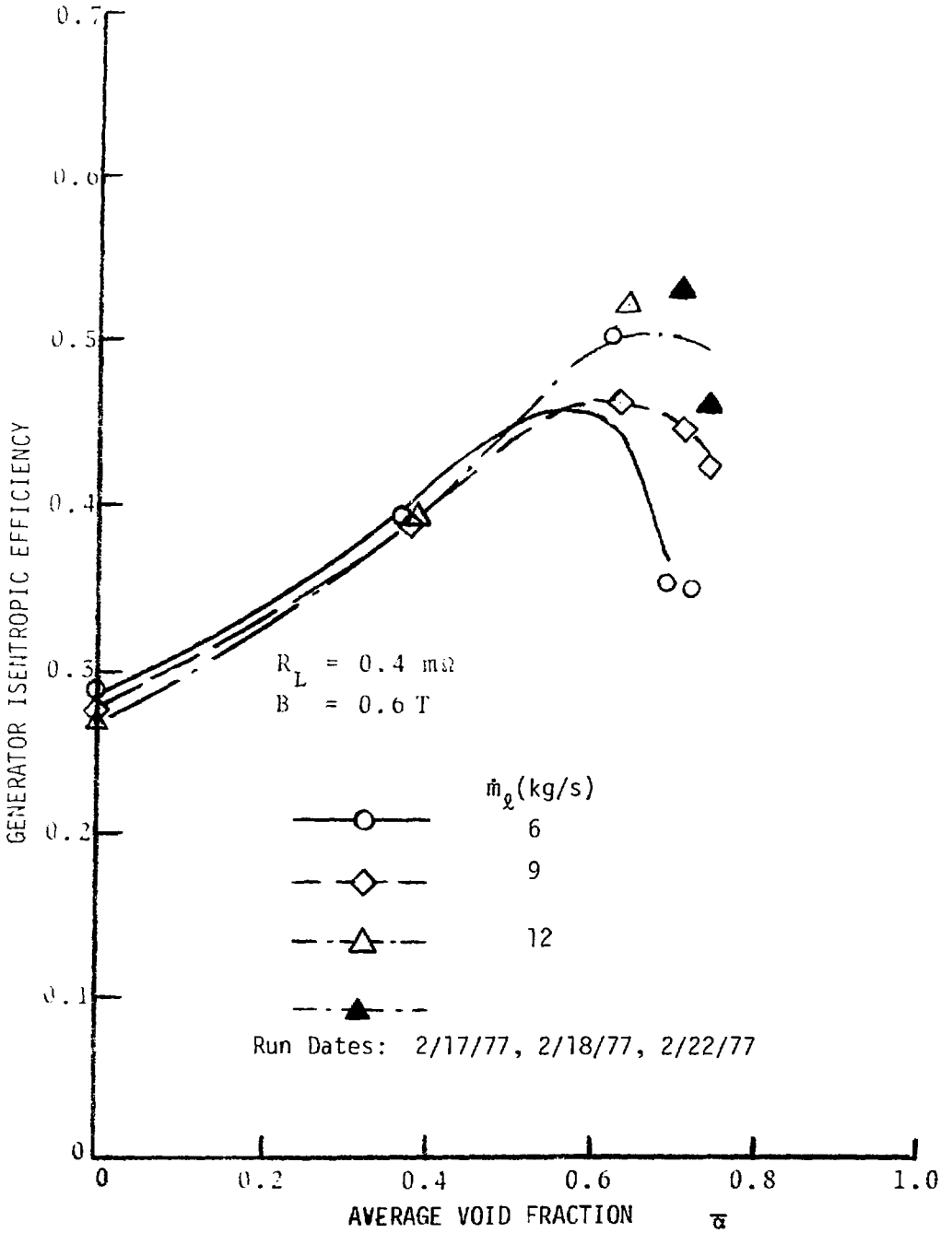

Figure III.13. Influence of Liquid Flow Rate on Generator Efficiency at B = 0.6T and R_L = 0.4mΩ

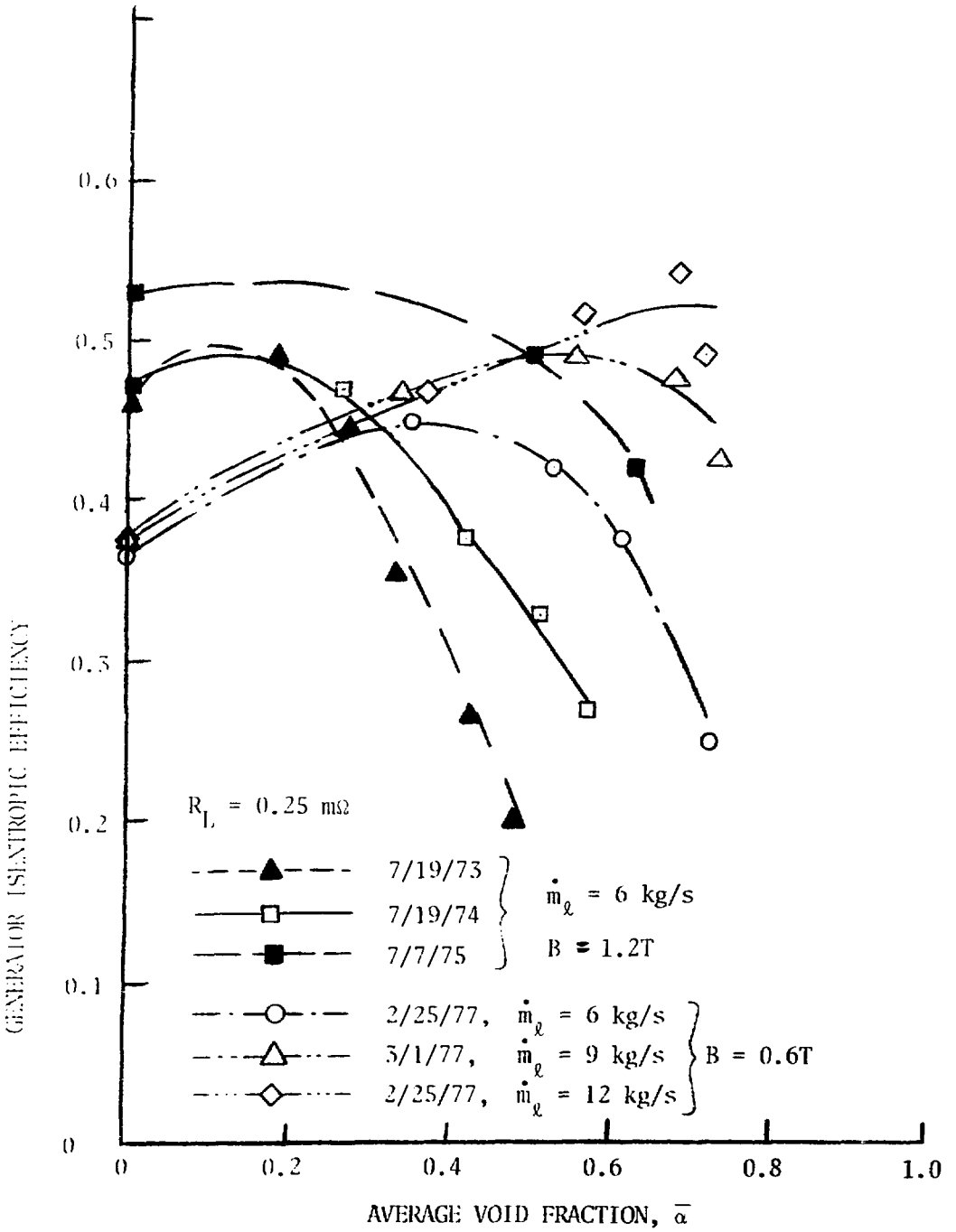

Fig. III.14 Comparison of ANL Generator Efficiencies for $R_L \simeq 0.25$ mΩ

the ratio of the inertial to gravity forces, where ρ is the liquid density, u_ℓ the liquid velocity, g the acceleration of gravity, and D_b the typical bubble length scale. For slug and churn-turbulent flows D_b is comparable to the hydraulic diameter of the channel. From this, increasing u_ℓ or decreasing D_b (smaller bubbles, foam or bubbly flow) yields higher values for Fr or lower slip ratios.

With two-phase MHD flows the Lorentz force replaces gravity as the dominant body force. Thus, it may be appropriate to define a magnetic Froude number as the ratio of the inertial to Lorentz forces, or

$$Fr_M = \frac{\rho u_\ell^2}{\sigma u_\ell B^2 (1 - F) D_b} \quad .$$

Here σ is the electrical conductivity of the two-phase mixture, B the magnetic flux density, and F the load factor (ratio of terminal voltage to generated voltage). From a qualitative examination of the existing data, slip appears to decrease as Fr_M increases. For example, previous MHD experiments have shown that the slip ratio decreases with increasing velocity, increasing load resistance (F in Eq. III.2), and decreasing pressure gradient.[3] (Note that Eq. III.2 does not include any effect of B on the effective bubble size. Also, the creation of a foam flow would decrease D_b by about two orders of magnitude, making the effect of the other variables on Fr_M and the slip ratio negligible.)

Measured average slip ratios as a function of the liquid flow rate (velocity) are shown in Fig. III.15 for 0.6 T and 0.14 mΩ. Each set of three runs for a given quality were made consecutively on the same day to minimize measurement effects. A definite, large decrease in the

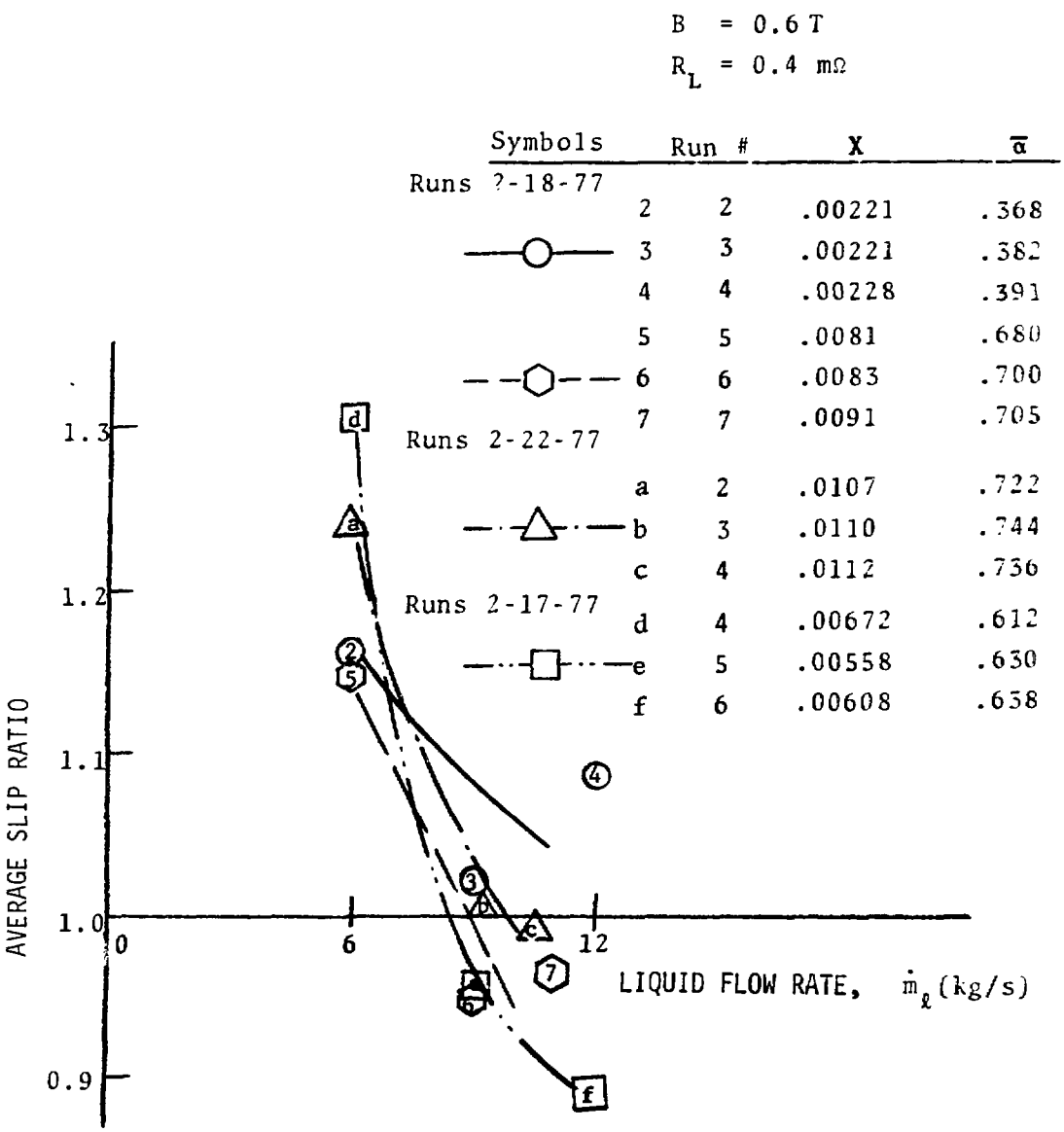

Figure III.15 Influence of Liquid Flow Rate on Average Slip Ratio

average slip ratio with increasing flow rate is apparent. (Average slip ratios less than unity are not expected, but are within the accuracy of the measurements. The accuracy limit does not affect the trends.)

The slip ratio, pressure, and void fraction variations along the generator are shown in Figs. III.16 to III.18 and III.19 to III.21 for the third and fourth data sets of Fig. III.15, respectively. Note the increase in the pressure gradient and the decrease in the slip ratio as the liquid flow rate increases. The change in the latter from 6 kg/s to 9 kg/s is particularly pronounced in both cases.

III.3 Liquid-to-Gas Heat Transfer

One of the key features of the LMMHD concept is the almost-constant-temperature expansion of the two-phase flow in the generator due to the high heat content of the liquid relative to that of the gas. (The liquid acts as an "infinite-reheat" source for the gas, thermal energy is continuously transferred from the liquid to the gas, and most of the enthalpy change in the generator comes from the liquid.) This almost-constant-temperature expansion is the major factor in the high thermodynamic efficiency of LMMHD power cycles. Realization of this expansion depends on effective interfacial heat transfer from the liquid metal to the gas, and thus it is necessary to check the adequacy of this interfacial heat transfer.

Analytical solutions for this heat transfer are of limited value because the details of the flow, such as bubble size, are unknown. Experimental measurements of the local gas and liquid temperatures in NaK is not within the present state of the art (see Section V.5). Thus, qualitative experiments were performed that show the existence of good heat transfer.

The experimental geometry is shown in Fig. II.1. The nitrogen and NaK temperatures at the mixer inlet and the nitrogen temperature exiting the

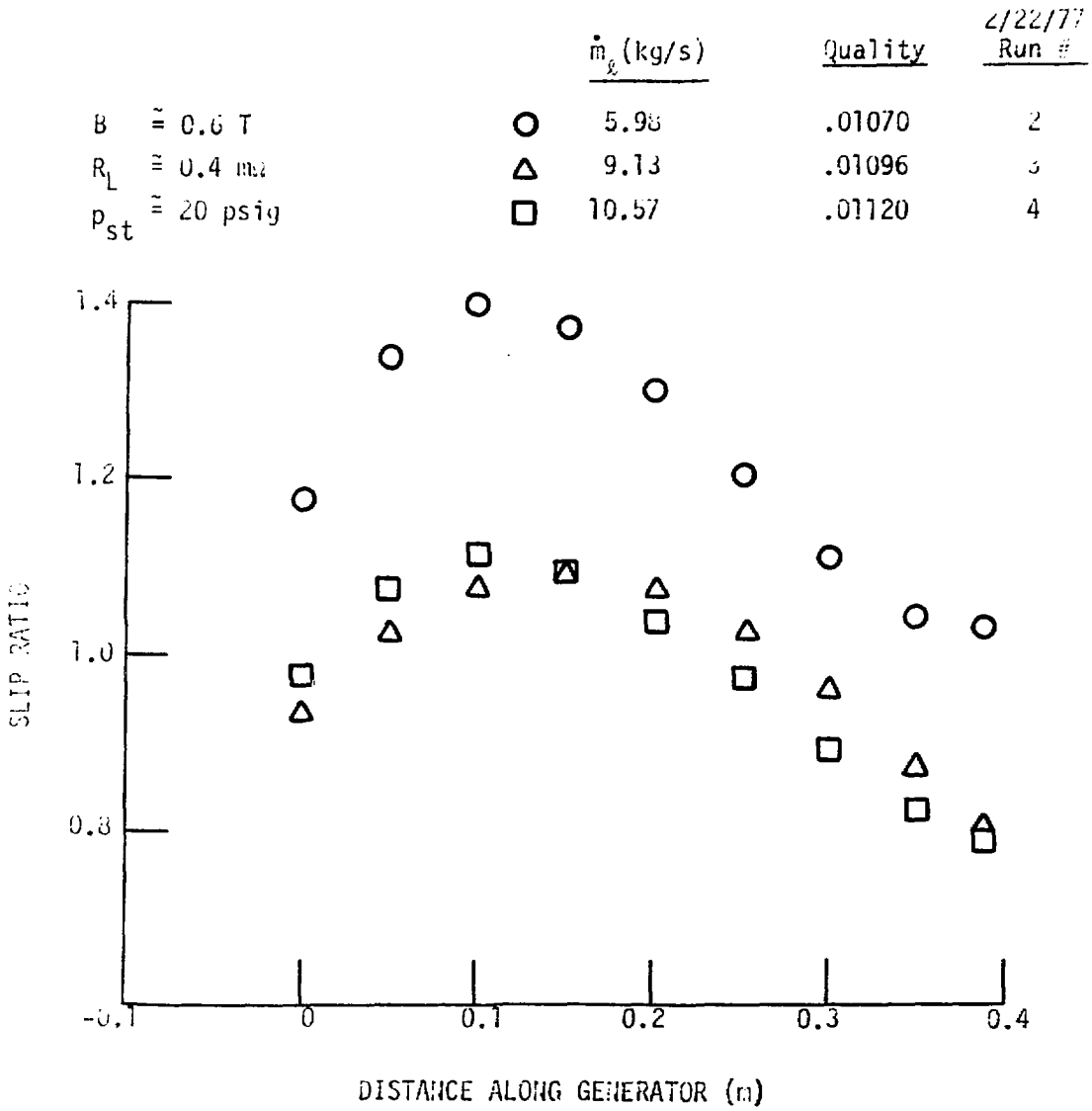

Figure III.16 Slip Ratios Along Generator, χ = 0.01

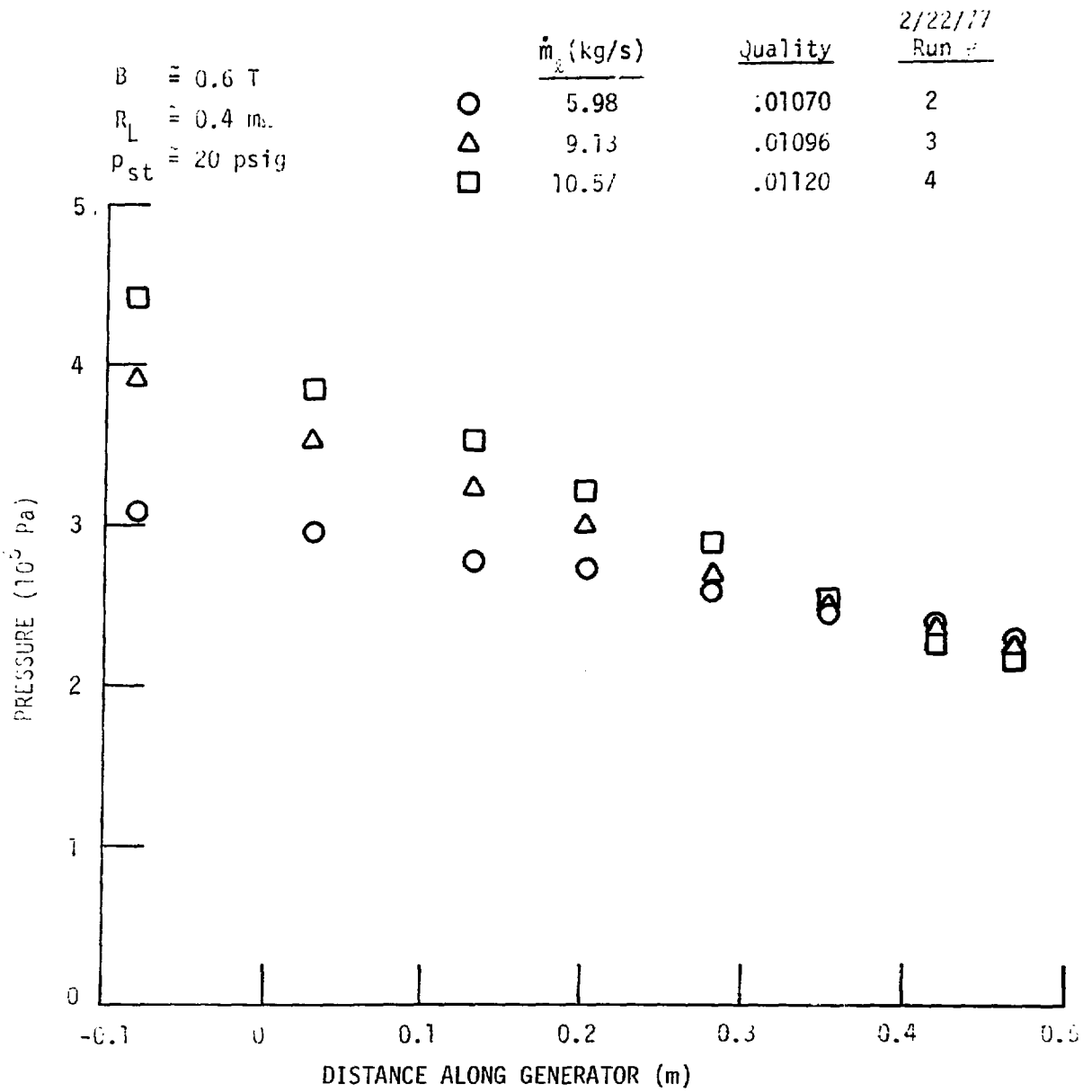

Figure III.17 Pressure Along Generator, χ = 0.01

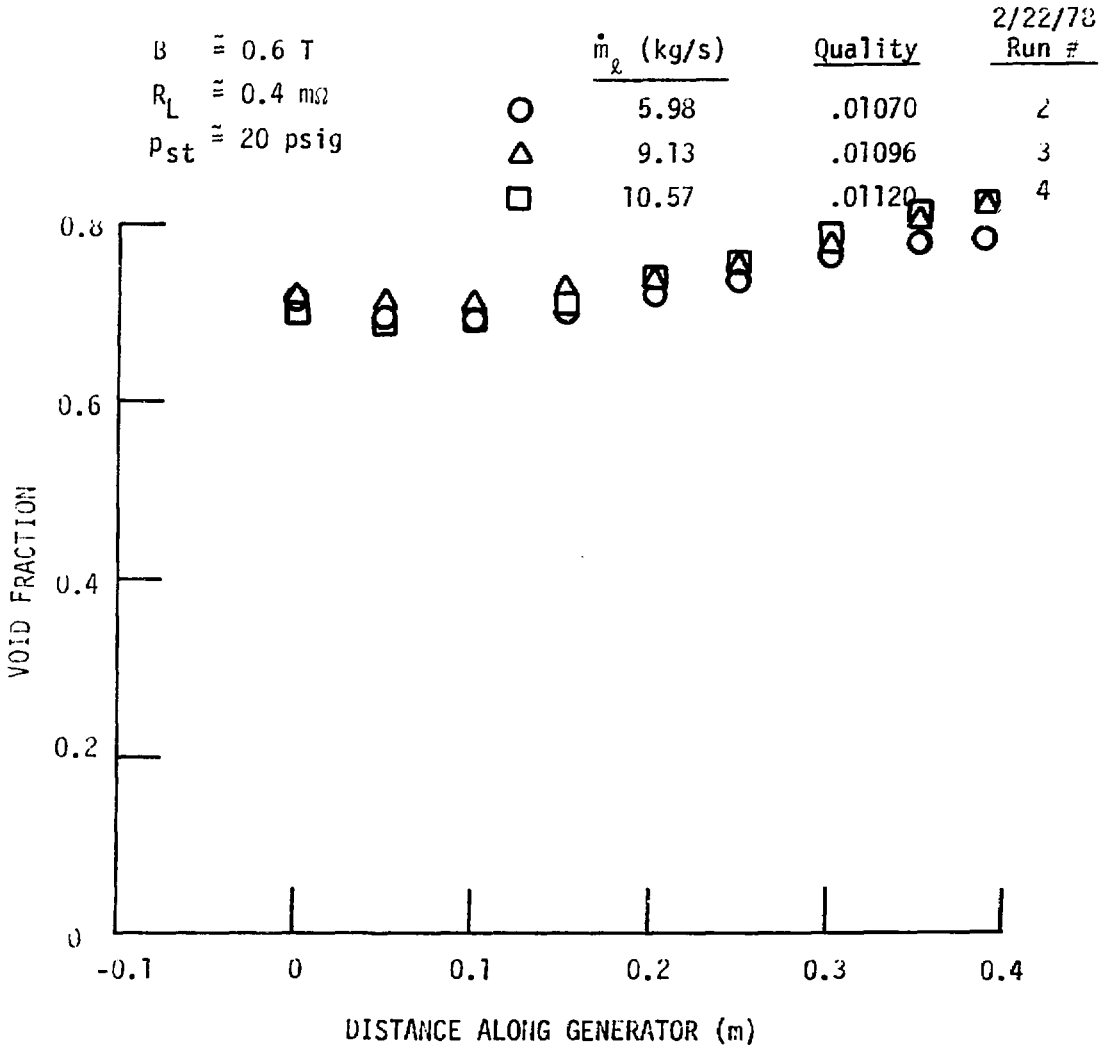

Figure III.18 Void Fraction Along Generator, λ = 0.01

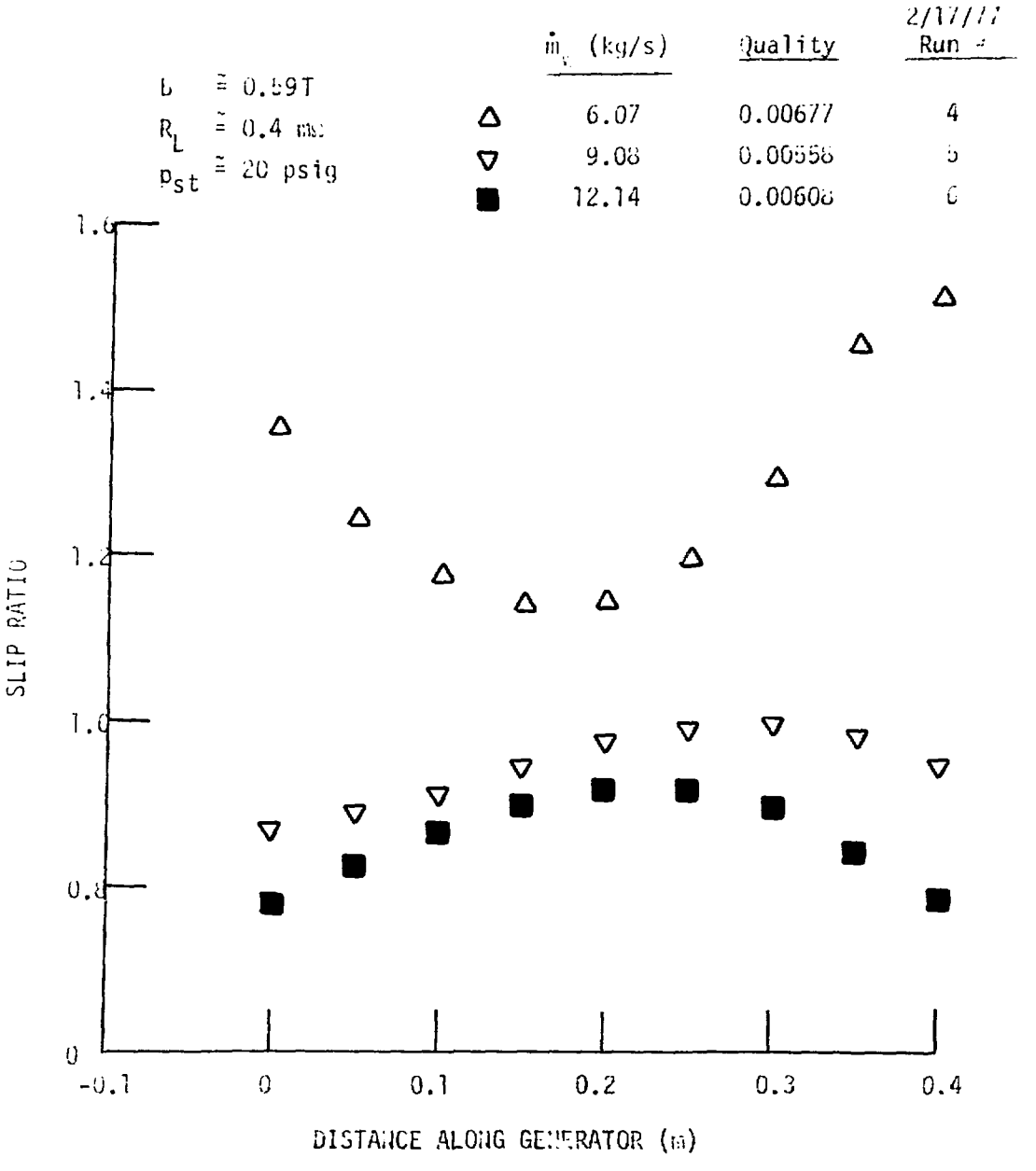

Figure III.19 Slip Ratios Along Generator, χ = 0.006

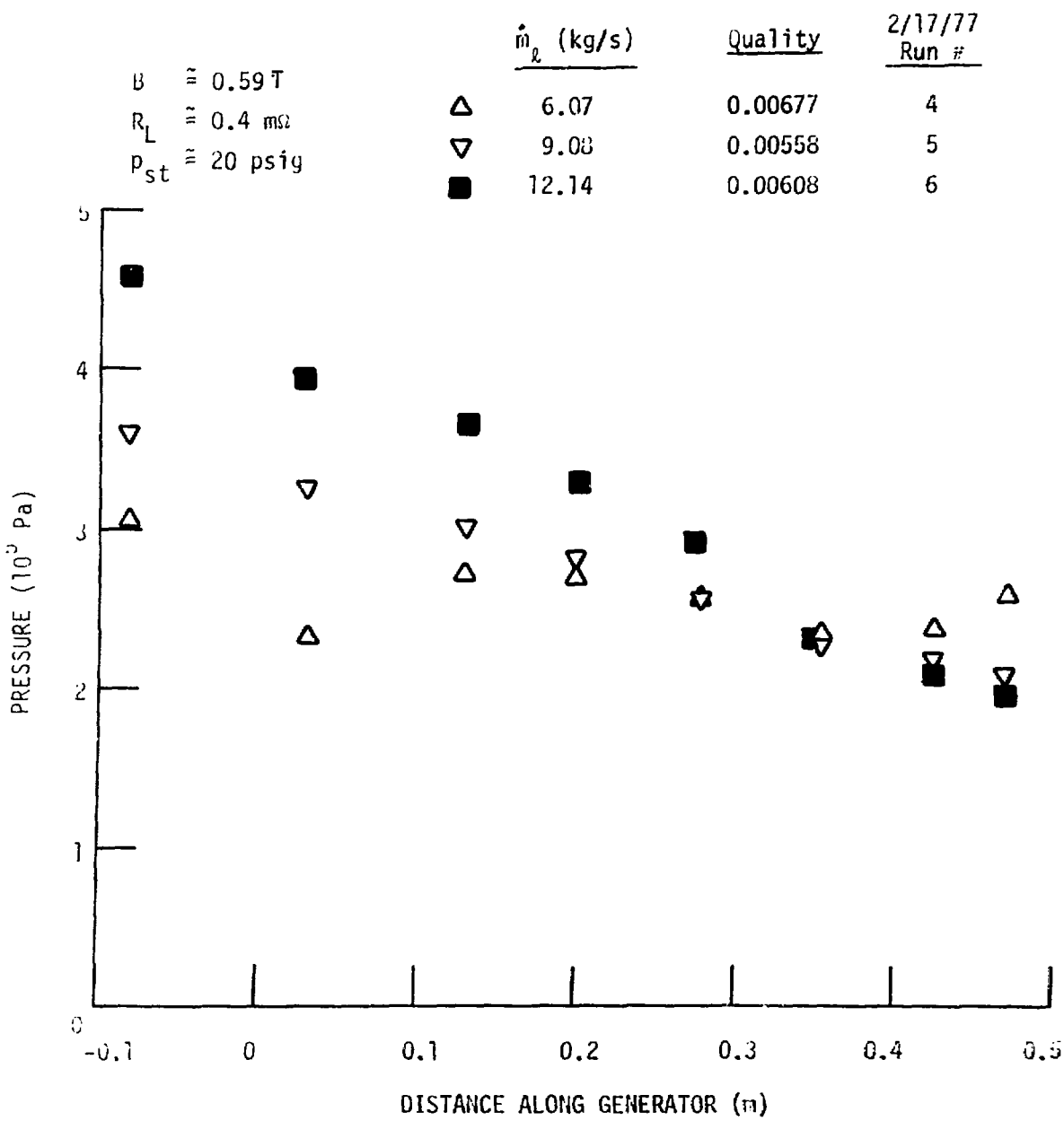

Figure III.20 Pressure Along Generator, x = 0.006

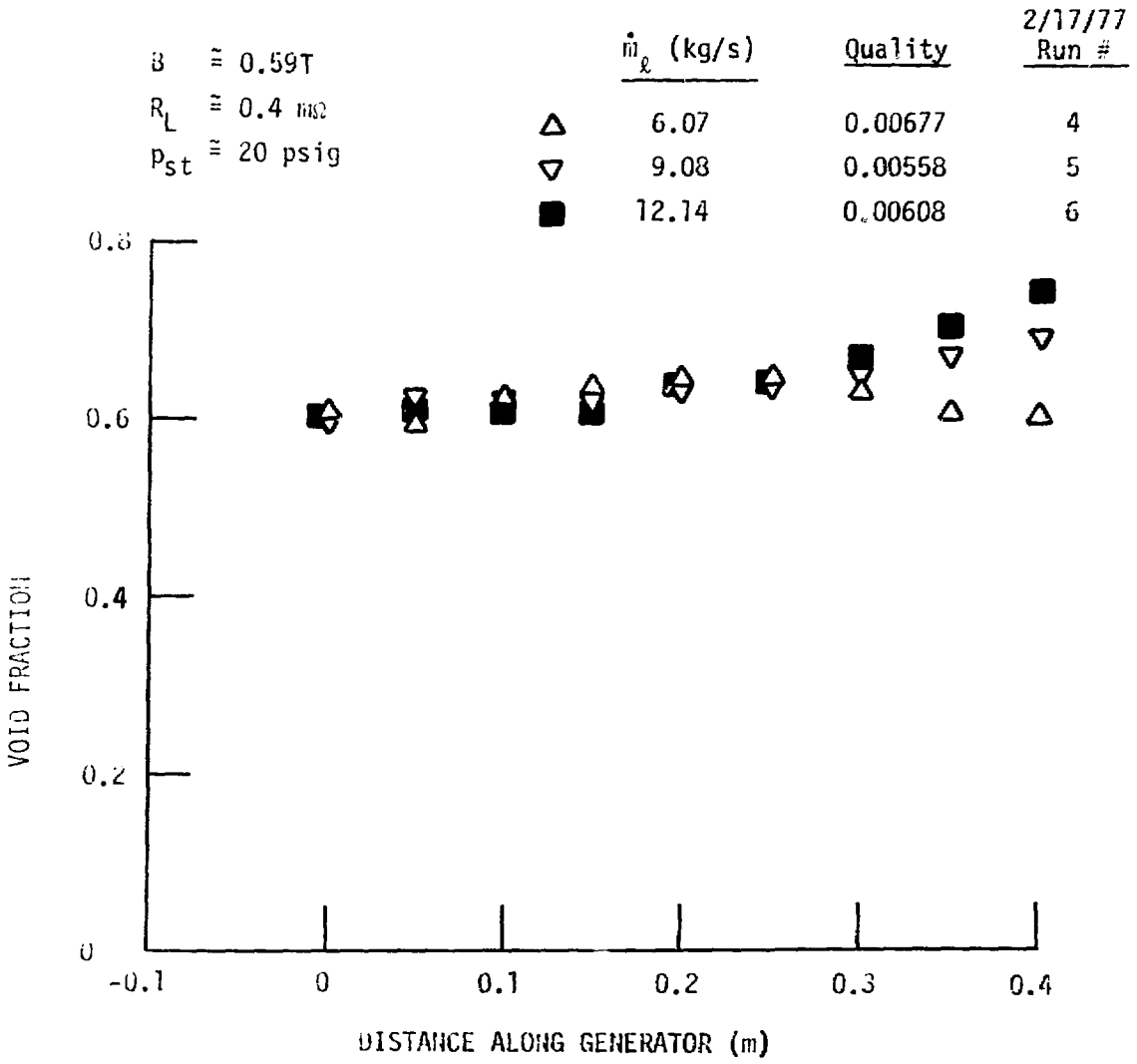

Figure III.21 Void Fraction Along Generator, χ = 0.006

separation tank are measured by means of thermocouples. The nitrogen exit temperature is measured in the six-inch exhaust pipe about 1.5 m downstream of the separation tank, and the distance from the generator exit to the separation tank is only about 0.6 m. Measurement of the NaK temperature downstream of the generator was not considered necessary because its temperature decrease is less than one kelvin (with perfect heat transfer, somewhat less with reduced heat transfer) if the nitrogen and NaK enter the mixer at the same temperature.

The results from one set of experiments are shown in Fig. III.22, where the nitrogen enters the mixer up to almost sixty kelvins cooler than the NaK and the run numbers indicate the time sequence. The NaK temperature increased with time because the loop was not cooled and the nitrogen inlet temperature decreased with time as the tank trailer cooled off, but these changes have no influence on the conclusions. The generator was electrically loaded, resulting in a high pressure drop across the generator, so that if the nitrogen expanded isentropically (i.e., without heat transfer from the NaK) to the generator exit pressure its temperature would decrease by about seventy kelvins. The data (Fig. III.22) shows that instead of cooling off, the nitrogen was heated to almost the NaK inlet temperature. (Note that the decrease in the NaK temperature in the generator and the decrease in the nitrogen temperature in the exhaust pipe due to its cooler surroundings are both in the direction such that, if corrected for, the actual exit temperature difference would decrease.) This data clearly shows that effective interfacial heat transfer exists, as required for the high thermodynamic efficiency of the LMMHD concept.

Data for cases where the nitrogen enters the mixer hotter than the NaK are shown in Fig. III.23. The nitrogen temperature is lower at the higher flow rates (qualities) because of the limited nitrogen heater power. Again, the exit temperatures are very close.

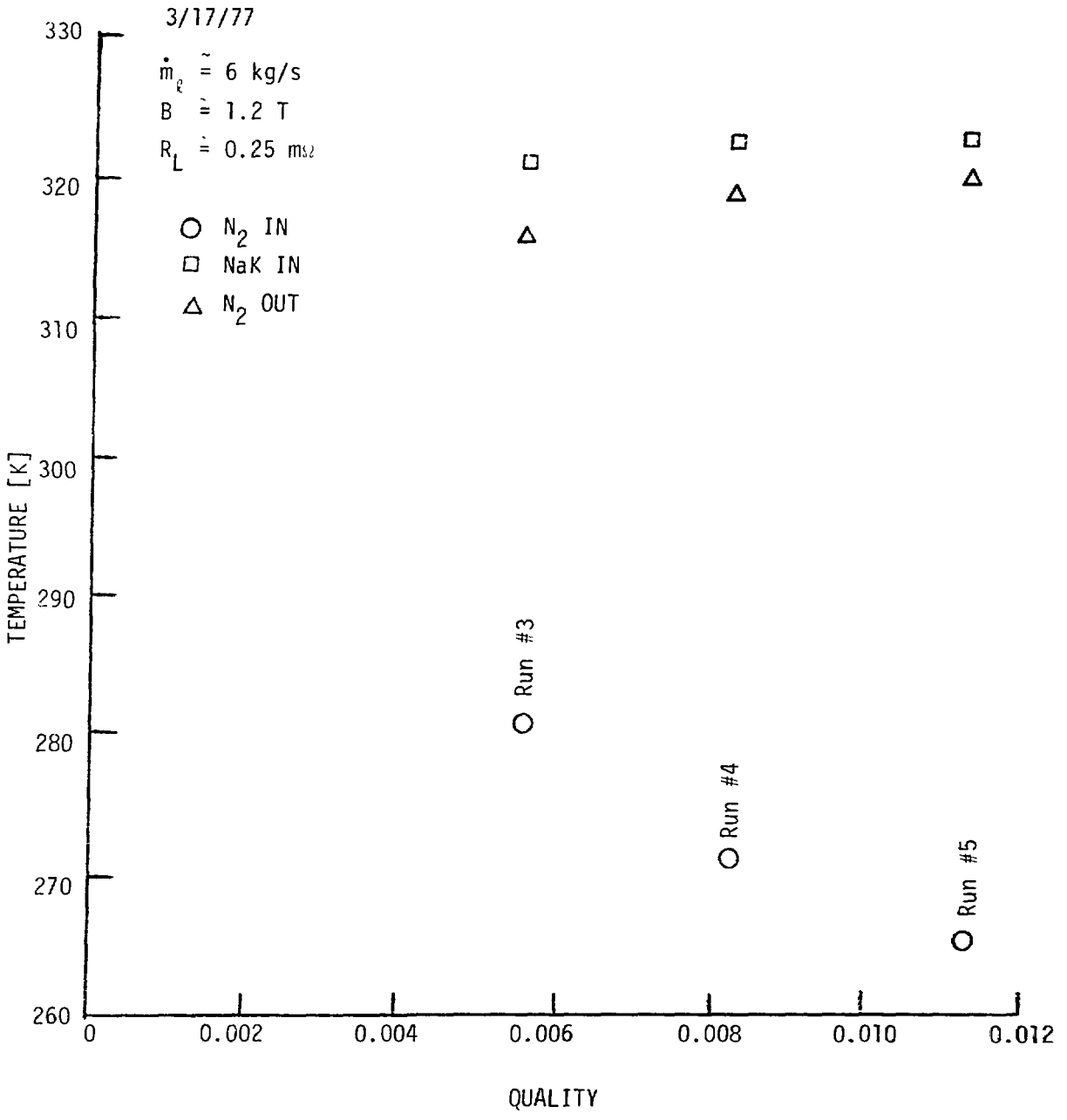

Figure III.22 Generator Experiments to Show Liquid-to-Gas Heat Transfer, Gas Enters Colder than Liquid

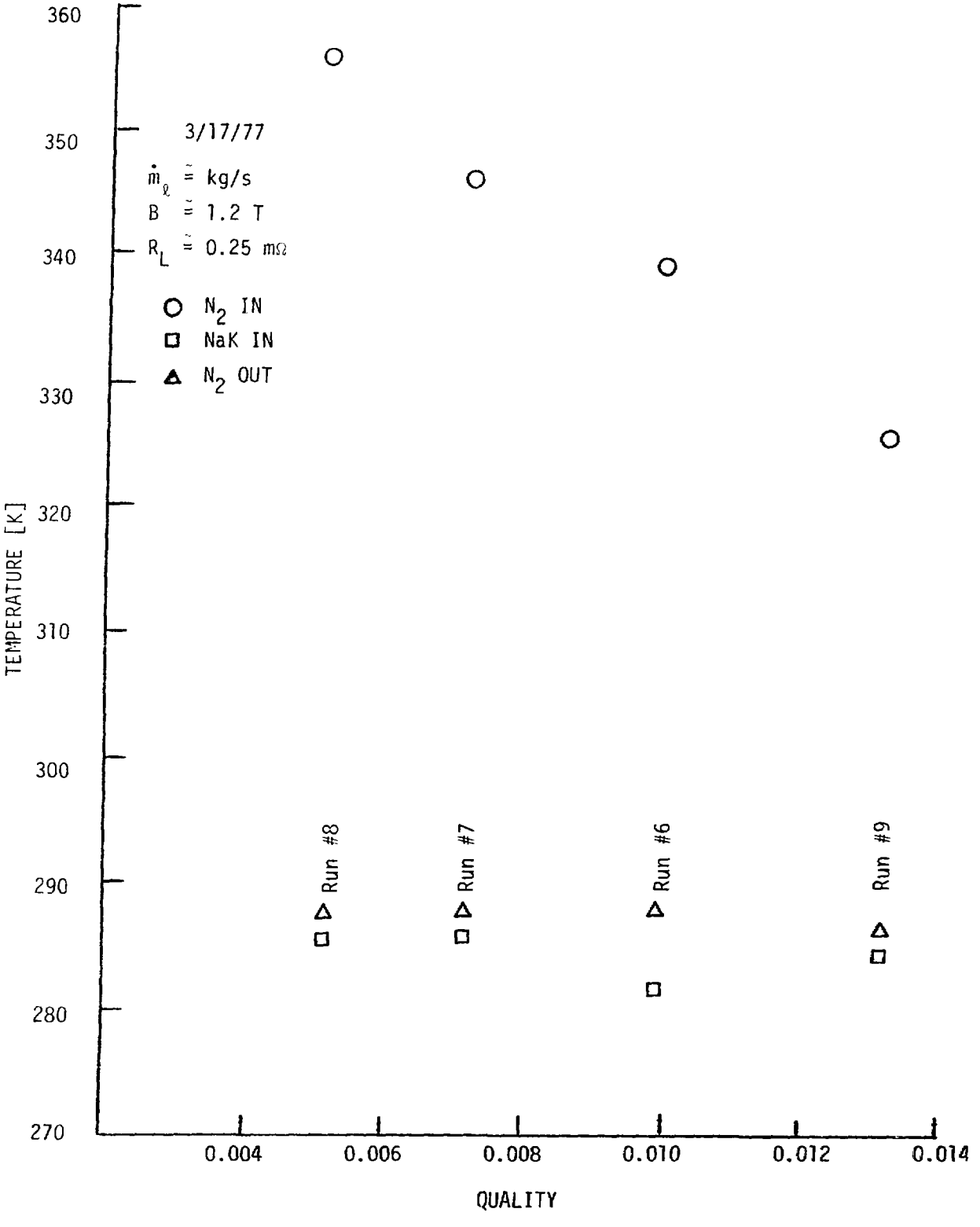

Figure III.23 Generator Experiments to Show Liquid-to-Gas Heat Transfer, Liquid Enters Hotter than Gas

III.4 Magnetic Field Shaping

Many of the experimental runs have large variations in the liquid velocity u_ℓ, and this results in circulating currents, non-constant pressure gradient along the electrode length, and extra losses.[4] This effect is particularly pronounced for single-phase liquid flow because of the diverging channel. To minimize the circulating currents it is best to keep the induced electric field $u_\ell B$ constant, and this requires a variable B if u_ℓ is not constant. This is particularly important for high generator efficiency where load factors close to unity are required.

Zero-quality MHD experiments were performed to see the change in performance if the magnetic field strength increased as the liquid velocity decreased. Small iron pieces were placed on the magnet poles to increase the magnetic field strength along the generator, as shown in Fig. III.24. The increase in magnetic field strength was only about one-seventh (measured by the averaged additional strength) of the ideal; however, the improvements in efficiency were 5 and 9 percentage points at $\dot{m}_\ell$ = 6 and 9 kg/s, respectively. (The efficiencies were 0.421 and 0.473 at 6 kg/s, and 0.369 and 0.457 at 9 kg/s.) The pressure profiles for the two 9 kg/s runs, Fig. III.24, show that the pressure gradient is more-nearly constant with the iron shaping.

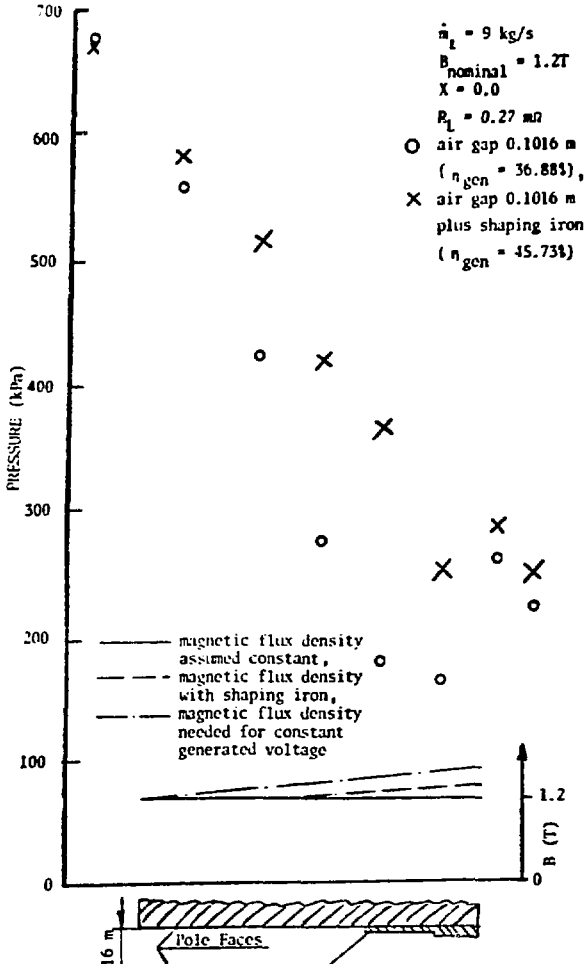

Figure III.24 Distributions of Magnetic Flux Densities and Pressure Along the Generator

IV. LIQUID-METAL FOAMS AND SURFACE-ACTIVE AGENTS

Despite the wealth of information on aqueous and organic foams, there is no broadly unifying theory, and there are many inconsistencies in the data and in the definition of foaminess. The liquid-metal medium differs greatly from the molecular water and organic systems, and it is not clear that a liquid-metal foam is a realistic expectation. Nevertheless, it is encouraging to note the patent literature describing the preparation of solid, foamed metal, which must have passed through a foamed quasi-liquid stage.[14,15] Wettable fine metal powders are described as essential foam promoters in such processes, apparently by virtue of the increased viscosity of the powder-bearing systems. Alternatively, as with aqueous and organic foaming systems, the surface properties of the liquid can be modified with dissolved materials. Thus, it appears attractive to investigate the utilization of both particulate and soluble agents that could aid in creating a liquid-metal foam when a gas is expanded through the liquid metal. This program is focussed on NaK alloy and is assessing various foam promoters by examination of foaminess, wettability, and surface tension.

IV.1 System Description and Experimental Approach

IV.1.1 Particulate Dispersions

Bubbles stabilized by particulate matter, also called three-phase foams, have been discussed by Bikerman.[16,17] In addition to increasing viscosity and, thereby, impeding film drainage, solid particles can have the effect of increasing the activation energy of bubble coalescence. The process can be visualized from Fig. IV.1, where a contact angle of 90° is assumed. The solid particle is in a bubble surface with gas on the left and liquid

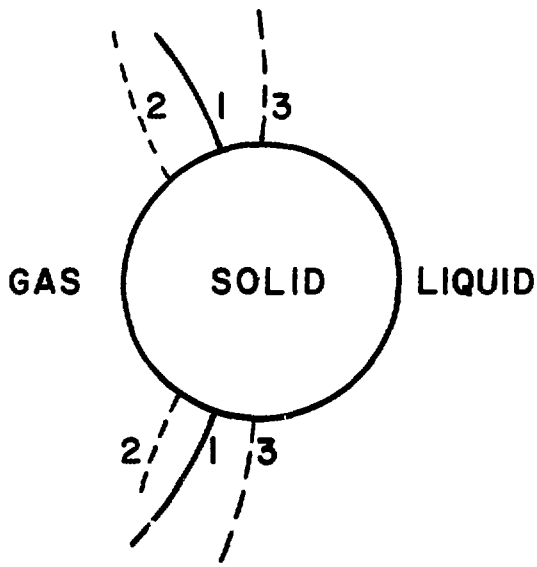

FIGURE IV.1.
THE EFFECT OF A SOLID PARTICLE ON A BUBBLE

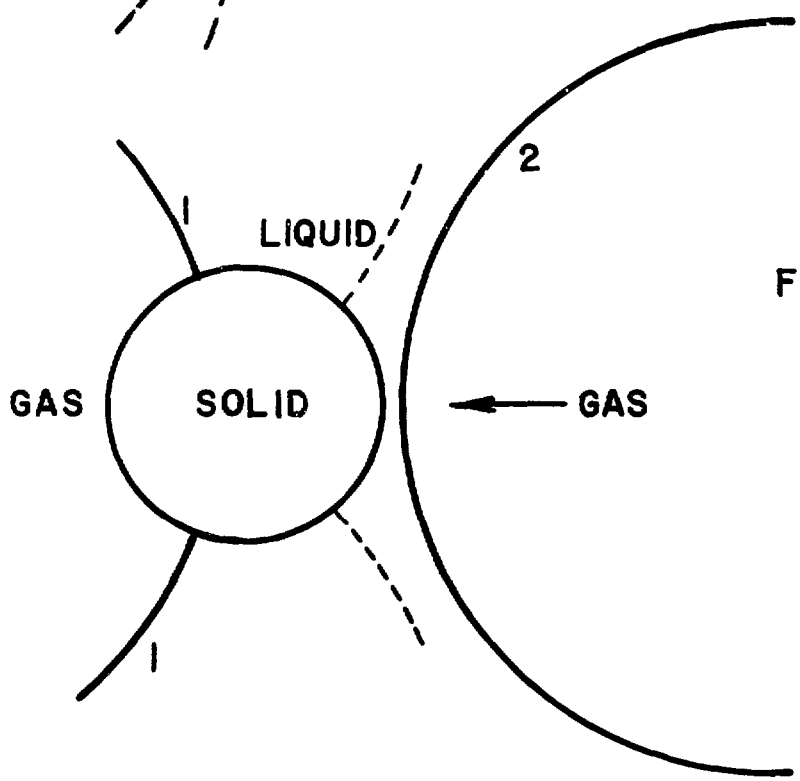

FIGURE IV.2.
POTENTIAL BUBBLE COALESCENCE

on the right, with position (1) being the stable, equilibrium position. For the particle to move out of the bubble to position two (2) would distort the bubble if the contact angle is to be maintained. Also, to move the particle into the bubble to position three (3) would distort the bubble out of its spherical, minimum energy configuration. Either motion is energetically unfavorable and is resisted. The potential coalescence with another bubble can be considered in terms of Fig. IV.2. For the second bubble to coalesce with the first, the solid particle must be incorporated into the bubble's surface and, at some stage, a 90° contact angle situation must be established, such as that shown by the broken line. The surface energy of the second bubble would have to increase, a requirement that would inhibit coalescence. Particle size, shape, and wettability would influence the amount of this coalescence activation energy.

Recent experience with the ambient-temperature NaK -nitrogen facility[6] appears consistent with a correlation between improved performance and the effect of particulate matter. The carbon steel loop was rusty when first assembled; thus, in time, iron oxide particles probably broke loose, became altered in wettability and size distribution so as to favor bubble stabilization, and, thereby, improved loop performance.

IV.1.2 Soluble Additives

In discussing the effect of adding soluble additives to NaK alloy as foam promoters, it should be noted that solutions of both surface-active and surface-inactive additives have been reported in the literature to exhibit foaminess. Because the term "surfactant" refers to surface-active materials, it is limiting to refer to the present program concerned with foaming NaK systems as a surfactant program. It is true, however, that more surface-active than surface-inactive foaming systems seem to have been

found, and that most theories of foaming are slanted toward consideration of the effect of surfactants.

Surface activity refers to the fact that solutions of certain solutes in a given solvent will show a lower surface tension than the pure solvent and that the surface layer contains a higher concentration of the solute than does the bulk solution. The mathematical relationship is given by the Gibbs adsorption isotherm:

$$\Gamma_2^1 = \frac{-c}{RT}\frac{d\gamma}{dc} \quad , \qquad \text{(IV.1)}$$

where Γ_2^1 is the excess concentration of solute 2 in the surface of the solution of solvent 1, c the bulk concentration of solute, γ the surface tension, R the gas constant, and T the absolute temperature. The value of excess concentration depends on the Gibb's definition of a surface. More exactly, in the equation above, Γ_2^1 is the excess number of moles of solute 2 in the surface over the number of moles of solute 2 present in a bulk region containing the same number of moles of solvent 1 as the surface. In effect, a mathematically-constrained plane must be visualized as defining a surface volume to fit this definition.

The relevance of surface tension relationships to foaming may be more readily understood by introducing Gibbs' expression for the property of surface elasticity as given by

$$E = 2d\gamma/d\ln A \qquad \text{(IV.2)}$$

or

$$E = 4(\Gamma_2^1)^2(d\mu_2/dm_2), \qquad \text{(IV.3)}$$

where A is surface area, μ_2 the chemical potential of the solute, and m_2 its amount per unit area of film. The elasticity is regarded

as a measure of a film's capacity to respond to periods of stress. Both Γ_2^1 and $d\mu_2/dm_2$ should be large to maximize elasticity. From the expression for Γ_2^1, it is apparent that large values of c and $d\gamma/dc$ are favorable. A preferred "large" value of c means the solubility of the solute should be appreciable; however, there is evidence that c attains an optimum value. In practice, m_2 is difficult to measure, so that the above reasoning serves more as a qualitative approach than as a quantitative guide.

As a further insight into foaming, there is the view that the rate of surface adsorption of a foam-stabilizing surfactant should be relatively low. The reasoning is that a sudden stretching of the film surface reduces the excess surface concentration of solute. Under such conditions, the local surface tension would tend to rise and, by virtue of the Marangoni effect, draw more liquid into the region to thicken and strengthen the film. However, should the surfactant diffuse-in too quickly, the surface tension would be lowered before the restorative flow of liquid could take place, and the weakness of the film would be prolonged.

These considerations provide a rationale for carrying out surface tension measurements in this program. In many of the cases that will be discussed, saturated solutions were dealt with as a practical necessity, because of the low solubility in NaK that most materials have at room temperature. This fact alone can explain the minimal bubble enhancement that was often found. In principle, examination of less-then-saturated systems is possible; however, this would have required the development of techniques for both preparing and analyzing solutions with solute concentrations at the parts per million level. The development of such a capability for each system individually would be costly, in time and money, and, therefore, was considered outside the scope of this exploratory program.

Hence, only saturated systems were dealt with in the cases discussed here.

IV.1.3 Experimental Approach

Preliminary experiments indicated that tests of bubble performance appeared to offer the best approach for surveying a variety of potential foam promoters. Although somewhat subjective, this test provides a common basis for comparing bubble or foam production and is related, in a simple way, to the actual LMMHD foam generating situation. The complex, imperfectly-understood interplay of variables in foaminess (e.g., surface tension, surface elasticity, surface dilational and sheer viscosity, bulk viscosity, and the atomic and molecular interactions underlying these effects) is believed to manifest itself in bubble tests of the type carried out.

However, to avoid a completely empirical and ad hoc study, some basic quantitative measurements pertinent to the foaming process were included. These are the measurement of surface tension for systems of soluble additives in NaK, and of bulk viscosity for systems of particulate dispersions in NaK. The technique being used for surface tension measurements is the Sugden two-tube form of the maximum bubble pressure method.[18] The bulk viscosity of particulate dispersions is measured by a commercial instrument, the Nametre vibrating sphere viscometer. Because it is difficult for some systems to wet the sphere of this viscometer, not all systems have been measured by this technique. Wettability plays a role throughout the experiments, even in the bubbling tests. As a result, some measurements of the contact angle (a measure of wettability) between NaK and various solid substrates as a function of treatment of the substrate were made by the Wilhemy plate method.

The maximum bubble pressure method was selected for the measurements of the surface tension of liquid metals. This method, often used on such

systems in the past, is well suited to remote measurements on opaque systems. Also, it is essentially insensitive to differences in contact angle once the orifices are wetted. Basically, the method consists of measuring the pressure inside a bubble that is blown at the end of a vertical capillary tube immersed in the liquid of interest. The measured pressure is composed of a portion caused by the hydrostatic head at the immersion depth and a portion caused by the surface tension forces in the bubble. By using two capillaries of different diameters immersed to the same depth, the hydrostatic contribution will be cancelled in the expression relating the surface tension to the pressures measured in the two tubes. This two-tube version is the Sugden method.[18] Sugden also introduced a treatment, which is being used in these studies, for the correction of the surface tension values for the non-sphericity of the bubbles.

IV.2 Results

IV.2.1 Wetting Aspects

Wettability is an important factor in bubble performance and in the stabilization of bubbles by particles and by soluble additives. Bubble performance was found to depend on orifice wetting. If the orifice was first wetted by rubbing it with a small drop of NaK-carbon black mixture, the bubbles produced were smaller and more numerous. There were indications that, even without carbon black, NaK could support bubble formation after the orifice had been wetted. In other tests, the orifice was first treated with a drop of warm hydrofluoric acid and then rubbed with NaK. In this instance, smaller bubbles and larger numbers of coexisting bubbles could then be blown.

Most bubble performance tests were run with a single, wetted orifice immersed in 18 cc of NaK contained in a Pyrex tube of 2.1 cm (0.83 in.) ID.

Multiple-orifice devices were tested, but were not adopted as the primary basis of evaluation. A tube with a single 0.051 cm (0.020 in.) orifice, another with three orifices of that size, and a tube with a 2-mm upturned glass frit, all wetted with carbon-black dispersion and run at a standardized flow rate of 5 cc/min, produced essentially the same bubble performance. Furthermore, with the single-orifice disperser in place and with the cross section of the tube containing NaK alloy reduced significantly, a bubble column (foam) 0.5 to 1 cm high was formed at a nitrogen flow rate of 50 cc/min. At 240 cc/min, the bubble column was approximately 5 cm high. Because the single orifice was capable of demonstrating the desired phenomena, it was adopted as part of the standard test. The variability in performance of the multi-orifice disperser or frits that is discussed in the literature could have introduced added complications and uncertainty in interpreting the results. Therefore, these devices were not utilized in the standard test.

With the difference in bubbling behavior for wetted and unwetted orifices having been established, it could be expected that differences in wetting at the gas-NaK mixer could be at least partially a cause of the observed differences in the pressure drop measured across the LMMHD generator.[6] In those tests, the higher pressure drop was correlated with reduced slip ratio in the NaK-nitrogen alloy system, presumably resulting from better or more bubbly (or foamy) flow.

In early tests of wettability, a drop of NaK was placed on the surface to be tested, and the tendency of the NaK to wet or to roll around easily was observed. The results of these tests are given in Table IV.1. Anodically cleaned surfaces of both carbon steel and stainless steel were found to be more easily wetted than those cathodically cleaned.

Table IV.1

Wetting Experiments--NaK on Carbon Steel and Stainless Steel

	Tab and Treatment	Wetting Results
1.	Type 304 stainless steel. Rinsed with CH_3OH	NaK drop had slight tendency to stick at first contact
2.	Carbon steel. Rinsed with CH_3OH	NaK drop was mobile.
3.	Stainless steel. Rinsed with dilute HCl, distilled H_2O, CH_3OH. Electrocleaned 60 s cathodically, 15 s anodically.	NaK drop was mobile.
4.	Carbon steel. Same treatment as 3.	NaK drop was mobile.
5.	Stainless steel. Electrocleaned as above, Cd plated, rinsed with H_2O and CH_3OH.	NaK drops stuck in one place.
6.	Carbon steel. Same treatment as 5.	Same as 5.

Cadmium-plated surfaces were wettable, and stainless steel was more wettable than carbon steel. Ease of surface wettability was: cadmium better than stainless steel better than carbon steel.

More quantitative comparisons of wettability were possible through the contact angle measurements. In such measurements, wetting is associated with a contact angle between 0° and 90°, and non-wetting with an angle between 90° and 180°. Contact angle measurements are, in general, not high precision measurements, but they provide information on trends of wetting. Contact angle hysteresis, a difference between the values of the advancing and receding angles (advancing larger than receding), is found almost universally and is seen as a symptom of a contaminated surface or of nonequiilbrium.

The results of the contact angle measurements are given in Table IV.2, and show that wetting for advancing angles was never achieved with any of the various treatments . However, in all but two cases, receding angles showed varying degrees of wetting. The two cases of non-wetting are believed to have resulted from the residual adsorption of the halide used in cleaning the tabs. Residual adsorbed basicity correlates with some degree of receding contact wettability. Prolonged exposure to NaK alloy leads to improved wettability, as shown by a decline in both advancing and receding contact angles. Also, NaK-carbon black mixtures show this effect, even though qualitative, visual observatrions indicated that wetting occurred. The contact angles for NaK-Vulcan XC-72R dispersion on stainless steel were surprisingly large at first, but swishing the steel sample in the liquid metal led to more extensive wetting. Time and mechanical stimulation tended to improve wetting on cadmium-plated surfaces. The superior wettability of type 304 stainless steel compared with carbon steel is demonstrated by the contact angle values. Nickel plating also favored

wetting; the lowest receding contact angle was found for a nickel-plated tab after soaking in NaK alloy.

From this work, it appears that gas injection orifices made of stainless steel rather than carbon steel should perform better in NaK LMMHD systems. Nickel plating appears to improve performance. However, other approaches to wetting may also prove effective and easier to implement, such as the use of soluble additives in NaK that both promote foam formation and act as wetting agents.

IV.2.2 Particulate Dispersions

IV.2.2.1 Carbon Blacks

D. R. Vissers[19] reported that a dispersion of a certain carbon black in NaK would wet glass and stainless steel at room temperature. This suggested that a suitable carbon black might be a foam promoter. Two carbon blacks were selected for examination; one, Monarch 1300 (Cabot Corp.), is quite similar to the Carbolac that Vissers used and the other, Vulcan XC-72R, is an electrically-conductive material. The ultimate particle sizes of these two carbon blacks range from 13 nm to 30 nm for the Monarch 1300 and the Vulcan XC-72R, respectively. In dispersing the carbon blacks, Vulcan XC-72R was wetted easily by the NaK and dispersed quickly, whereas Monarch 1300 tended to float on the surface of the NaK and required prolonged stirring for good dispersion. Both mixtures did wet glass and stainless steel, and both favored bubble formation and bubble retention. For Monarch 1300, a 4.7 wt % dispersion seemed to give the best bubble performance. Similar behavior was found for the Vulcan XC-72R systems in the concentration range of 0.55 to 3.1 wt %. More highly concentrated mixtures for both systems gave the kind of bubble performance that would be expected for a viscous medium, i.e., slowly emerging bubbles in a slowly flowing liquid.

Table IV.2

Contact Angle Measurements in NaK (eutectic) Alloy

	Tab and Treatment	Contact Angle, degrees Advancing	Receding
1.	Stainless steel. Electrocleaned cathodically and anodically, rinsed, dried overnight at 180°C (455 K)	141-157	58-70
2.	Stainless steel. Electrocleaned cathodically and anodically, rinsed, barely dried before being placed in vacuum port.	157-161	54-68
3.	Stainless steel. Electrocleaned, plated with cadmium, rinsed, dried briefly.	180	98,79,74, 58 in sequence
4.	Stainless steel. Polished with emery paper, electrocleaned, plated with nickel, rinsed, and put in vacuum port while still wet with CH_3OH	157-171	34-45
5.	Same tab as #4 but after soaking in NaK for 50 min. Streaks of NaK wetness remain on tab.	138-172	13-43
6.	Stainless steel. Polished mechanically, electrocleaned cathodically and anodically, rinsed, put in port wet. Tested with NaK-Vulcan XC-72R mixture (~2%)	158-168 Mechanical simulation leads to wetting.	60°
7.	Carbon steel. Polished mechanially under isopropyl alcohol, rinsed, and put in port wet.	156-168 Visibly uneven contact angle.	71-99
8.	Same tab as #7 but after soaking 1 hr 45 min in NaK.	138-146	67-73
9.	Carbon steel. Electrocleaned anodically 1 min per side, rinsed, put in port wet.	161-174	61-85
10.	Carbon steel. Electrocleaned anodically 40 min per side, rinsed, put in port wet.	139-155	42-79 (47 median)

Table IV.2 (Cont'd)

11.	Carbon Steel. Electrolyzed 10% KCl solution with tab as anode, rinsed, put in port wet	~180	~180
12.	Carbon steel. Polished mechanically, rinsed, cleaned ultrasonically in 15% hydrofluoric acid, rinsed, put in port wet.	~180	~180
13.	Carbon steel. Polished mechanically, cleaned ultrasonically in Na_2CO_3-NaOH-Na_3PO_4 cleaning solution, rinsed, put in port wet.	122-132	59-60
14.	Carbon steel. Polished mechanically, cleaned ultrasonically in Na_3PO_4 solution for 25 min per side, rinsed, put in port wet	140-150	55-65
15.	Carbon steel. Same tab as #14 but stirred in NaK for 2 h	132-140	40-47

Viscosity changes appeared to contribute to bubble enhancement in the carbon black systems. Measurements of the viscosity-density product (which is the unit of readout of the viscometer) were made on NaK with 1.5 wt % Vulcan XC-72R. There was some experimental difficulty with variable wetting of the viscometer sphere, but there does appear to be a definite increase in viscosity at room temperature, i.e., 7.9×10^{-4} Pa·s for pure NaK and about 1.6×10^{-3} Pa·s for the NaK-carbon black system. This particular NaK-carbon black sample was able to produce about four coexisting bubbles at the standard flow rate of 5 cc/min in a bubble test, and supported a bubble bed about 1 cm high at 50 cc/min. Higher flow rates did not increase the height of the "foam."

Settling of carbon-black dispersions is a possible problem if the dispersions are to be used in a LMMHD loop. Measurements were made of the extent of settling of a 1.04 wt % Vulcan XC-72R dispersion after standing undisturbed for 68 days. Near the bottom of the column, the dispersion contained 3.3 wt % carbon, whereas the top of the column contained only 290 ppm carbon. If particulate dispersions are ever adopted for flow homogenization in a LMMHD machine, and if the settling is troublesome, consideration will have to be given to means for maintaining the most fully dispersed condition during shutdown periods or for re-dispersing settled material by a special start-up process.

The surface tension of a 1.2 wt % Vulcan XC-72R dispersion was measured and found to be the same as that of pure NaK. (The surface tension data are summarized in Table IV.3.) This result supports the proposition that the demonstrated effectiveness of carbon black in promoting bubble lifetime and foaminess in NaK involves a viscosity increase that could retard film drainage and/or an increase in the bubble coalescence activation energy.

The enhanced wettability of stainless steel and Pyrex in contact with NaK-carbon black mixtures probably results from the adhesion of a wettable (and wetted) layer of carbon black to the steel or glass surface.

IV.2.2.2 Titanium and Cadmium Powders

Experimentation on stabilization of bubbles by particulate materials included tests with finely divided metals, namely titanium and cadmium, both of <200 mesh (<74 μm). With titanium, progressive additions of the powder gave mixtures that showed modest enhancement of bubble formation and an increased tendency to wet stainless steel and Pyrex. However, this wetting tendency was not as great as that found with the Vulcan XC-72R carbon black. With cadmium powder, effects similar to that with titanium were observed. In this case, however, there could have been some superimposed surface activity effects; cadmium is known to depress the surface tension of NaK.

IV.2.2.3 Oxygen-Containing Additives

It was thought that molecular, as well as atomic species were surface active and might, also, augment surface elasticity by virtue of their orientation in the surface film. Alkoxides, OR^-, the organic anion portion of an alcohol, were tested. Methoxide and n-butoxide were formed in NaK by additions of small quantities of methyl alcohol or n-butyl alcohol. Solubilities were very low; thus, saturated solutions of these species were most-easily prepared. The surface tensions were not depressed. A similar result was obtained with hydroxide introduced into the NaK by adding a small amount of water. In the case of butoxide, a bubble test showed improved bubble performance. This improvement might have been due to stabilization of bubbles by butoxide particulate matter, rather than by

surface activity effects. With methoxide, bubble performance was not improved significantly.

IV.2.2.4 Potassium Bromide

Bromide ion is a fairly large, polarizable ion that was thought might be surface active in NaK. However, a mixture of KBr in NaK did not depress the surface tension, perhaps because of its low solubility at room temperature. Yet, tests of bubble performance showed some improvement in bubble longevity over that of NaK alone.

IV.2.3 Soluble Additives

IV.2.3.1 NaK Alloy Eutectic

For an accurate perspective, it is worth noting that, if surfactancy correlates with foaming tendencies, some bubble stabilization in pure NaK might be expected. For pure one-component systems, the common understanding is that foaming is impossible. However, NaK is a two-component system and, even if devoid of low-level surfactant impurities, it is self-surface active. This characteristic is established by the surface tension isotherms for the sodium-potassium system, published by Bradhurst and Buchanan,[20] which indicate that potassium is surface-active in sodium.

Bubbling tests on "pure" NaK provided somewhat variable results, depending on the extent of orifice wetting. With an unteated orifice, fairly large bubbles would break through the surface and burst immediately. With orifices wetted by rubbing with a small amount of NaK-carbon black, smaller and more numerous bubbles formed, a situation that is taken to reflect the innate surfactancy of NaK. As a result, a somewhat variable reference point for comparing bubble performance with pure NaK existed. For the systems that are regarded as promising, however, the performance

was clearly better than that observed on even the favorable end of the range of bubble formation for pure NaK.

For measurements at ambient temperatue, the surface tension of NaK drawn from a large source [90.7 kg (200 lb) drum], on different occasions, seemed to vary from 0.114 to 0.122 N/m (Table IV.3). The average value is taken to be 0.118 $\pm$ 0.003 (one standard deviation) N/m. NaK that had been stored in contact with carbon black for 4 1/2 months showed a higher surface tension, 0.132 N/m, suggesting that the freshly-drawn NaK contained surface-active impurities that were removed by gradual adsorption on the carbon black surface. NaK freshly prepared from sodium and potassium showed a surface tension of 0.111 to 0.113 N/m. From the lot analyses of the purchased NaK and of the sodium and potassium used for the fresh preparation, it seems reasonable to presume that silicon and magnesium impurities (up to 33 and 12 ppm, respectively) are surface-active in NaK. Experimentation to confirm this hypothesis is planned.

IV.2.3.2 Sodium Additive

Though done at elevated temperatures, the Bradhurst and Buchanan[20] work on surface tensions in the sodium-potassium system suggests that other compositions in this system may have a more favorable surface tension situation for bubble formation than the eutectic NaK composition presently being used. [The eutectic composition in the sodium-potassium system is 66 mol % (or 76.7 wt %) potassium.] The experimental composition is 77.17 wt % potassium, and will be designated NaK 77 in this section. The phase diagram for the sodium-potassium system shows that compositions from 43 to 87 wt % potassium are liquid at 295 K (20°C). To determine whether a different NaK composition might offer an advantage for use in LMMHD, a mixture of 44.3 wt % potassium (designated NaK 44) was prepared.

The surface tension was considerably lower than that of NaK 77, namely 0.071 N/m vs. 0.118 N/m. This value is close to that for water, 0.072 N/m. NaK 44 also resembles water in bulk viscosity, having a viscosity of 10^{-3} Pa•s while NaK 77 has a viscosity of about 7 x 10^{-4} Pa•s. The electrical resistivity of NaK 44 is known to be less than that of NaK 77, and this is an advantage in a LMMHD machine. Without any additives, NaK 44 appeared more prone to wet stainless steel than NaK 77. Under standard bubbling test conditions with a wetted orifice, it developed persistent bubbles more quickly than NaK 77, and somewhat more of them. It may be well to keep in mind the possible advantages for the LMMHD machine of the use of NaK 44 (or other compositions in the sodium-potassium system that have not yet been explored).

IV.2.3.3 Cadmium

A carbon-black dispersion which was found to have the same surface tension as NaK was used as the solvent to prepare a 0.12 wt % (0.025 mol %) solution of cadmium in NaK. The surface tension was depressed to 0.103 N/m, from an initial value of 0.122 N/m. Cadmium is known to be surface active in sodium; at 575 K it depresses the surface tension of sodium about 10% at a concentration of 4 mol %.[16] In the present NaK system, the depression is approximately 16% at 0.25 mol %. The apparently greater impact on NaK is probably a result of mainly the lower temperature of the NaK system. Enhanced bubble performance was observed for a 0.21 wt % solution of cadmium in NaK.

IV.2.3.4 Sulfur

Sulfur was found to be surface active in NaK, depressing the surface tension by about 35% of its value in the absence of sulfur.

The sulfur was added in the form of pure anhydrous Na_2S (0.12 wt % Na_2S = 0.051 wt % S). Not all of the added Na_2S dissolved, and the solubility of sulfur in NaK at room temperature is not known. Thus, the observed surface tension resulted from a saturated solution with a concentration of less than 0.051 wt % sulfur. In the bubbling test, bubble performance appeared somewhat better than in the absence of sulfur.

IV.2.3.5 Selenium

Selenium was found to be about as surface active as sulfur. The added amount, 0.13 wt %, was in excess of the solubility of selium in NaK, i.e., it did not all dissolve. Compared to sulfur, bubble performance with selenium seemed somewhat more favorable for foaming. At a flow rate of 80 cc/min, a bed of bubbles two to three bubbles high was formed.

IV.2.3.6 Cesium

Cesium is somewhat surface active in NaK. In the concentration range 0.0114 wt % (0.0029 mol %) to 0.23 wt % (0.058 mol %) cesium, the surface tension goes through a minimum. The lowest value found was at 0.11 wt % (0.028 mol %); the reduction was about 10% of the original value for NaK. That the surface tension goes through a minimum is not unusual. For example, the surface tension-composition curve for the sodium-potassium system itself shows a minimum, as does the curve for the thallium-mercury system. Bubble promotion for the 0.11 wt % system was unimpressive.

Table IV.3

Surface Tension Measurements on NaK 77 Systems at Room Temperature

ID No.	Description	Surface Tension, N/m
1	NaK 77 (eutectic) at room temperature	0.122
2	Sample 1 3 h later	0.122
3	NaK 77 with 1.2 wt % carbon black (Vulcan XC-72R) 1 h after mixing	0.122
4	Sample 3 18 h after mixing	0.122
5	Sample 4 with 0.12 wt % cadmium added, 1 h after stirring at room temperature, dissolution not complete	0.122
6	Sample 5 heated (to 50-60°C) and stirred for 1/2 h, cooled, let stand overnight	0.120
7	Sample 6 four days later	0.103
8	NaK 44 (44 wt % potassium)	0.071
9	Sample 8 17 h later	0.071
10	NaK 77 that was stored in Pyrex vessel for three months	0.127
11	Sample 10 4 h later	0.128
12	Sample 11 four days later	0.128
13	Pure NaK 77 previously used only for contact angle measurements, uncontaminated	0.129
14	Sample 13 one day later	0.130
15	Sample 14 with 0.12 wt % Na_2S (equivalent to 0.051 wt % S, but not all soluble) four days after preparation	0.084
16	NaK 77 with 0.94 wt % Vulcan XC-72R carbon black, aged 4 1/2 months	0.132
17	Sample 16 after remaining quiescent in tensiometer for one month	0.141

Table IV.3 (contd.)

ID No.	Description	Surface Tension, N/m
18	Sample 17 after clearing orifices of tensiometer	0.131
19	Initially pure NaK 77 sample that acquired contamination, perhaps alkoxide	0.046
20	Sample 19 three days later	0.050
21	Pure NaK 77	0.119
22	Sample 21 3 h later	0.120
23	Sample 22 with 0.13 wt % Se (but not all soluble)	0.072
24	Sample 23 one day later	0.082
25	Pure NaK 77	0.114
26	Sample 25 1 h later	0.113
27	Sample 26 with 0.0114 wt % Cs (0.0029 mol %)	0.112
28	Sample 27 21 h later	0.118
29	Pure NaK 77	0.114, 0.113
30	Sample 29 with 0.0114 wt % Cs (0.0029 mol %)	0.112
31	Sample 30 21 h and 43 h later	0.118, 0.117
32	Sample 31 with 0.106 wt % Cs (0.028 mol %)	0.106
33	Sample 32 3 h later	0.108
34	Sample 33 with 0.23 wt % Cs (0.058 mol %)	0.115
35	Sample 34 2.5 h later	0.117
36	Sample 35 2 h later	0.113

Table IV.3 (contd.)

ID No.	Description	Surface Tension, N/m
37	Pure NaK 77 freshly prepared from sodium and potassium	0.112
38	Sample 37 20 h later	0.113
39	Same material after partial oxidation by exposure to deteriorated glove box atmosphere over weekend	0.114
40	Sample 39 16 h later	0.115
41	Same material with CH_3OH (methanol) added	0.115
42	Sample 41 1.5 h later	0.117
43	Sample 42 18 h later	0.116
44	Same material with H_2O	0.112
45	Sample 44 2.5 h later	0.112
46	Same material with KBr (potassium bromide)	0.113
47	Sample 46 after weekend	0.113
48	Sample 47 after heating	0.113

V. CONCLUSIONS AND FUTURE WORK

Testing of the second diverging-channel generator (LT-3) with the revised ambient-temperature NaK-N_2 facility has been completed. The primary goal of the revised facility, demonstrating reduced slip ratio (ratio of gas velocity to liquid velocity) with higher liquid velocity (flow rate), was accomplished. The reduction in slip ratio, present in all cases, was dramatically demonstrated by a series of consecutive runs with varying flow rate (from 6 kg/s to 12 kg/s for the liquid). (Consecutive runs were made to minimize measurement effects.) Substantial increases in isentropic generator efficiency were obtained with higher liquid flow rates, an increase of more than 10 percentage points at the higher void fractions for a change to 9 kg/s from 6 kg/s.

Good liquid-to-gas heat transfer in the LMMHD generator is essential for a high-efficiency LMMHD power cycle, otherwise the expansion of the gas in the generator will not occur at almost constant temperature. Experiments showed that, even when the nitrogen entered the mixer more than 60 K hotter or cooler than the NaK, the two-phases of the flow exited the generator at essentially the same temperature; thus, the expansion at almost constant temperature was occurring.

The feasibility of generating relatively-stable bubbles and, hence, a foam, in liquid metals has been demonstrated. In mercury, cesium is a surfactant that markedly promotes bubble formation. In NaK, cadmium is similarly surface active. Photographic documentation of these phenomena was made in both motion and still pictures. Foamability was also demonstrated in a different kind of system, namely, a dispersion of carbon black in NaK. Surface tension measurements showed that the carbon black did not alter the surface tension of the NaK, thereby indicating that viscosity

(which was measured and found to have increased) is also a factor in promoting bubble formation and persistence (however, because of settling, carbon black appears unsuitable for LMMHD). Measurements of surface tension on NaK-S have shown sulfur to be surface active in NaK, and bubble formation is somewhat enhanced for this system. The surface tension of NaK with 44 wt % potassium was measured and found to be significantly lower than the eutectic NaK (77 wt % potassium) used in the rest of the experimentation and in the NaK loop. (There is an inherent surfactant mechanism in the NaK system itself, in that potassium is surface active in sodium. Conceivably, optimum foamability might be obtained with a system other than eutectic NaK.)

Contact angle measurements were made for stainless steel and carbon steel immersed in eutectic NaK. Non-wettable surfaces were produced by cleaning procedures using halogen-containing media, e.g., anodic electrolytic cleaning in KBr solution. Freshly nickel-plated surfaces were relatively wettable. The contact angle measurements showed that surfaces that were uniformly wettable to a fair extent, when freshly cleaned, became blotchily wettable after exposure to dust-free air. Wettability relates to the favorable performance of orifices in generating bubbles and foam, an effect demonstrated in laboratory tests with single-orifice bubblers.

An analytical study has placed limits on the shunt (wall) liquid layer thicknesses and losses, and this will provide guidelines for future generator experiments and designs. For large LMMHD generators, i.e., those with Hartmann numbers in excess of 1000, this loss represents a decrease of less than 1.0% in generator efficiency.

The desired next steps in the liquid-metal MHD program are described below.

V.1 Higher Velocities and Pressures

The design and most of the fabrication of the new test section--mixer, generator channel, and exit section--to utilize the full flow and pressure capacities of the loop has been completed. The generator, LT-4 of Fig. I.1, is designed to use the full loop capability of 10.9 kg/s and 1.48 MPa absolute. The channel will be installed in the loop, a test plan prepared, and generator performance measured over a range of load resistances and generator exit pressures or pressure ratios. Depending on the results from these tests, one or more new channel liners and exit sections with different tapers (area ratios) may be tested. The different tapers would fit different pressure ratios (or gas-to-liquid velocity ratios for surfactant tests). The results of the high-velocity high-pressure tests will be used to plan future generator experiments.

V.2 Foams

The first year's effort has demonstrated very positively the ability to generate foamy NaK at room temperature. However, the factors that operate to make this possible need to be identified and measured. Consequently, the continued testing of surfactants in NaK will have as one focus the selection of the most promising surfactants for foam promotion; sufficient attention will be given to the fundamental properties of the system (i.e., surface tension and viscosity) to provide a basis for correlating these properties with foamabilty and, thereby, developing some capability to predict bubble performance. The second focus will be on bubbling tests with foamy NaK.

The correlation effort will be pursued on two levels. A ranking of surface activity as a function of chemical nature of the surfactant

(i.e., by position in the periodic table and by molecular structure) will be formulated, analogous to the correlations that have been made for surface tension effects of various solutes in iron and other metals. In a somewhat more detailed fashion, calculations will be made of excess surface solute concentration, based on surface tension data and the chemical activity of the solutes. A relationship between surface tension and surface fraction of solute (which necessarily involves the atomic sizes) will be sought. For dilute solutions of surfactants, this may prove to be an adequate correlation device.

One primary difficulty is related to exploration of surfactant phenomena in NaK at room temperature: the typically low solubility of most solutes (surfactants). Determination of solute concentrations at such low levels is difficult, and, therefore, precise differences may be difficult to distinguish over the narrow range of solubility that exists. Practically, it becomes a matter of making measurements on pure NaK and then on saturated s_ ems. To improve the accuracy of the correlations, and, therefore, predictive capability, it is planned to extend these measurements to higher temperatures, where solubilities are greater. Further, higher-temperature measurements are also needed because conclusions based only on room-temperature data cannot necessarily be expected to be binding for conditions encountered in higher-temperature LMMHD systems.

Recent measurements have made it clear that surface tension is not the only determinative variable in promoting foaming. Observations suggest that viscosity is very influential in these systems, thus, this variable should be explored further.

Wetting properties, as measured by contact angles, will be examined for NaK in contact with stainless steel that has received various surface treatments. Pure NaK, as well as surfactant-containing NaK, will be

utilized. An objective will be to recommend conditions of NaK composition and solid substrate treatment that are most favorable for loop operation. This will mean optimizing both wetting and non-wetting situations, as required by different portions of the loop.

V.3 End Effects

End effects in liquid-metal MHD generators can be a significant loss mechanism, especially because the coupling between increased terminal voltage and increased end loss limits the attainable voltage in high-efficiency generators. Thus, a better understanding of end losses is required for the improvement of generator performance. An evaluation of methods to minimize the total end loss will be initiated. The points to be considered are: 1) the effect of the number and the length(s) of the insulating vanes on the electrical (ohmic) end loss, 2) the effect of the number and the length(s) of the insulating vanes on the viscous loss in the end regions, and 3) the effects on points 1 and 2 of the fringing magnetic field. The desired result is the identification of a method of minimizing the total end loss (electrical plus viscous) by varying the number and length(s) of the insulating vanes and the shape of the fringing magnetic field.

V.4 Imperfect Compensation

A one-dimensional and a two-dimensional model and code are under development. Both codes will use a circuit model to determine the compensation current distribution. The two codes will be run for cases corresponding to the existing generator experiments and to proposed practical generators. Limits on the effect of nonuniform compensation on generator performance will be established, and experiments to verify the model(s) planned and performed.

V.5 Improved Local Diagnostics

The experimental generator measurements include, at present, only macroscopic parameters--average void fraction, pressure at discrete points, liquid and gas mass flow rates, and terminal voltage and current. Improved two-phase flow diagnostics are required for determination of the local flow parameters--velocities, bubble sizes, pressures, and temperatures--needed for the generator model development, because the models use the local flow parameters.

Initial tests have been made with hot-film and resistivity probes in an air-water loop as part of the program to study two-phase LMMHD mixers, and special electronics have been developed for the resistivity probes. Following the completion of these air-water tests, tests will be made with the NaK-N_2 generator. The initial emphasis will be on single- and multiple-contact resistivity probes, because they will yield local void fractions directly, and bubble sizes and velocities through correlation techniques. Hot-film probe tests will be constrained by possible wetting (drift) problems and velocity (structural) limits. For both probes, it will be advantageous to record the signals and process them digitally.

REFERENCES

1. L. C. Pittenger, E. S. Pierson, R. Cole, and M. Petrick, "Experimental Two-Phase Liquid-Metal MHD Generator Program," Report No. ANL/ETD-72-07, Argonne National Laboratory, Argonne, IL, June 1972.

2. W. E. Amend, R. L. Cole, J. C. Cutting, and L. C. Pittenger, "Experimental Two-Phase Liquid-Metal Magnetohydrodynamic Generator Program," ANL/ENG-73-02, Argonne National Laboratory, Argonne, IL, June 1973.

3. M. Petrick, R. L. Cole, J. C. Cutting, W. E. Amend, and G. Fabris, "Experimental Two-Phase Liquid-Metal Magnetohydrodynamic Generator Program," ANL/ENG-75-02, Argonne National Laboratory, Argonne, IL, January 1975.

4. M. Petrick, G. Fabris, R. Cole, R. Hantman, E. Pierson, and J. Cutting, "Experimental Two-Phase Liquid-Metal Magnetohydrodynamic Generator Program," ANL/ENG-76-04, Argonne National Laboratory, Argonne, IL, November 1976.

5. M. Petrick, W. E. Amend, E. S. Pierson, and C. Hsu, "Investigation of Liquid-Metal MHD Power Systems," Report No. ANL/ETD-70-12, Argonne National Laboratory, Argonne, IL, December 1970.

6. M. Petrick, G. Fabris, E. S. Pierson, D. A. Carl, A. K. Fischer, and C. E. Johnson, "Experimental Two-Phase Liquid-Metal Magnetohydrodynamic Generator Program," ANL/MHD-77-3, Argonne National Laboratory, Argonne, IL, September 1977.

7. M. Petrick, P. F. Dunn, E. S. Pierson, and P. Lykoudis, "Liquid-Metal MHD Energy Conversion," ANL/MHD-78-5, July 1978.

8. C. C. Chang and T. S. Lundgren, "Duct Flow in Magnetohydrodynamics," ZAMP, 12, pp. 100-114, 1961.

9. P. F. Dunn, "Single- and Two-Phase Magnetohydrodynamic Pipe Flow," to be published.

10. R. W. Lockhart and R. G. Martinelli, "Proposed Correlation of Data for Isothermal Two-Phase, Two-Component Flow in Pipe," Chem. Eng. Prog., 45, pp. 39-48, 1949.

11. V. F. Vasil'ev, B. G. Karasev, and I. V. Laurent'ev, "Experimental Investigation of a DC MHD-Generator," Magnitnaya Gidrodinamika, 3, pp. 105-108, 1967.

12. A. I. Bertinov, and D. A. But, "The Effect of the Magnetic Reynolds Number on One-Dimensional MHD Flows," Magnitnaya Gidrodinamika., 3, pp. 71-76, 1967.

13. A. M. Winslow, "Numerical Solution of the Quasi-Linear Poisson Equation in a Non-uniform Triangle Mesh," J. Computational Physics, pp. 149-172, 1966.

14. D. M. Albright, W. R. Chilcott, Jr., and T. R. Floridis, U.S. Patent 3,360,361 (12/26/67) assigned to U.S. Steel Co.

15. J. A. Ridgway, Jr., U.S. Patent, 3,297,431 (1/10/67) assigned to Standard Oil Co.

16. J. J. Bikerman, Surface Chemistry-Theory and Applications, 2nd Ed., p. 376, Academic Press, New York 1958.

17. J. J. Bikerman, Foams, p. 149, Springer-Verlag, New York, 1973.

18. S. Sugden, J. Chem. Soc., p. 858, 1922.

19. D. R. Vissers, Argonne National Laboratory, private communication, 1969.

20. D. H. Bradhurst and A. S. Buchanan, Austral. J. Chem., 14, 397 1961.

APPENDIX A

SUMMARY OF EXPERIMENTAL GENERATOR DATA

OCTOBER 1976 TO SEPTEMBER 1977

Date	Run Number	Mass Flow Rate NaK $\dot{m}_\ell$ [kg/s]	Mass Flow Rate N_2 $\dot{m}_g$ [kg/s]	Magnetic Flux Density B [T]	Load Resistance R_L [mΩ]	Load Voltage V_L [V]	Pressure Inlet P_{in} [psia]	Pressure Exit P_{out} [psia]	Power Output P_e [kW]	Average Void Fraction $\bar{\alpha}$
10-11-76	1	12.14	0	0	∞	0	90.5	97.2	0	0
	2	12.05	0	.341	∞	.272	91.1	92.4	0	0
	3	12.05	0	.666	∞	-	92.2	80.5	0	0
	4	12.05	0	.966	∞	.776	92.2	53.1	0	0
	5	12.05	0	1.213	∞	-	95.6	38.2	0	0
10-12-76	1	6.07	0	1.25	∞	.483	58.7	35.2	0	0
	2	6.07	0	.975	∞	.391	50.8	34.4	0	0
	3	6.11	0	.65	∞	.258	41.3	33.9	0	0
	4	6.11	0	0	∞	.003	31.8	33.5	0	0
	5	6.11	0	.257	∞	.124	34.7	33.8	0	0
10-27-76	1	0	0	0	∞	0	-	-	0	0
	2	2.97	0	0	∞	0	-	-	0	0
	3	6.07	0	0	∞	0	-	-	0	0
	4	9.08	0	0	∞	0	-	-	0	0
	5	7.60	0	0	∞	0	-	-	0	0
	6	14.84	0	0	∞	0	-	-	0	0
	7	18.53	0	0	∞	0	-	-	0	0
	8	21.04	0	0	∞	0	-	-	0	0

Date	Run Number	Mass Flow Rate NaK $\dot{m}_\ell$ [kg/s]	Mass Flow Rate N_2 $\dot{m}_g$ [kg/s]	Magnetic Flux Density B [T]	Load Resistance R_L [mΩ]	Load Voltage V_L [V]	Pressure Inlet p_{in} [psia]	Pressure Exit p_{out} [psia]	Power Output P_e [kW]	Average Void Fraction $\bar{\alpha}$
12-10-76	1	6.025	0	-	∞	.495	74.9	35.8	0	0
	2	9.0153	0	-	∞	.747	97.5	36.3	0	0
	3	6.025	0	-	∞	.498	77.0	37.5	0	0
12-9-76	1	6.0027	0	-	.281	.474	76.5	36.7	0	0
	2	9.892	0	-	.272	.779	102.8	39.1	.800	0
	3	8.948	0	-	.272	.689	98.8	32.3	2.231	0
2-4-77	1	12.05	0	0	∞	0	19.1	20.5	0	0
	2	6.07	0	1.204	∞	.475	56.8	31.3	0	0
	3	6.07	.02182	1.197	∞	.754	50.0	31.2	0	.254
	4	6.025	.03280	1.197	∞	1.006	50.5	32.5	0	.450
	5	6.070	.4601	1.2	∞	1.196	51.0	32.4	0	.559
	6	6.070	.06065	1.192	∞	1.275	52.4	32.4	0	.587
2-7-77	1	6.070	0	1.212	.270	.471	73.3	34.8	.882	0
	2	6.025	.01385	1.22	.272	.468	74.2	34.2	2.382	.248
	3	6.093	.03369	1.205	.270	.818	72.8	30.1	2.478	.436
	4	5.971	.04907	1.205	.270	.865	73.7	37.5	2.771	.529
	5	6.043	.06770	1.212	.269	.933	74.0	30.1	3.236	.598
	6	5.98	.08832	1.20	.272	.992	76.2	30.0	3.618	.666
2-11-77	1	6.16	0	1.219	.399	.477	67.6	37.0	.570	0
	2	6.07	.01756	1.207	.408	.670	68.1	37.2	1.000	.296
	3	5.98	.03282	1.207	.429	.826	67.5	33.1	1.590	.478

Date	Run Number	Mass Flow Rate NaK $\dot{m}_\ell$ [kg/s]	Mass Flow Rate N_2 $\dot{m}_g$ [kg/s]	Magnetic Flux Density B [T]	Load Resistance R_L [mΩ]	Load Voltage V_L [V]	Pressure Inlet P_{in} [psia]	Pressure Exit P_{out} [psia]	Power Output P_e [kW]	Average Void Fraction $\bar{\alpha}$
2-11-77 (cont'd)	4	6.025	.04421	1.207	.410	.897	68.1	33.1	1.962	.578
	5	5.98	.06654	1.22	.407	.982	71.4	32.7	2.369	.654
	6	6.07	.08890	1.211	.406	1.100	75.8	32.5	2.980	.720
2-14-77	1	9.08	0	1.229	.399	.706	89.0	33.0	1.251	0
	2	9.01	.02778	1.200	.407	1.223	88.7	30.2	3.675	.263
	3	9.08	.03882	1.208	.404	1.398	91.5	30.4	4.838	.365
	4	9.08	.05510	1.210	.401	1.497	92.5	28.5	5.588	.506
	5	8.99	.04505	.830	.401	1.098	68.0	32.2	3.006	.571
	6	21.67	0	0	∞	0	28.5	32.2	0	0
2-17-77	1	6.02	0	.592	.387	.224	42.5	32.8	.130	0
	2	9.04	0	.592	.390	.338	46.7	32.2	.293	0
	3	12.10	0	.595	.389	.454	49.4	29.7	.530	0
	4	6.07	.04105	.588	.403	.515	44.3	37.3	.658	.612
	5	9.08	.05096	.588	.402	.867	52.3	30.3	1.870	.630
	6	12.14	.07431	.593	.401	1.300	66.2	28.3	4.214	.638
2-18-77	1	6.03	0	.585	.395	.239	47.2	35.0	.145	0
	2	6.07	.01345	.588	.395	.347	44.7	33.8	.305	.368
	3	9.17	.01937	.585	.397	.573	48.8	31.3	.827	.382
	4	12.14	.02777	.585	.399	.775	53.0	29.2	1.521	.391
	5	6.07	.04974	.585	.401	.591	48.7	34.0	.871	.686
	6	9.04	.07651	.585	.400	1.008	57.8	31.2	2.540	.703
	7	10.93	.10014	.586	.399	1.348	66.7	29.6	4.554	-

Date	Run Number	Mass Flow Rate NaK $\dot{m}_\ell$ [kg/s]	Mass Flow Rate N_2 $\dot{m}_g$ [kg/s]	Magnetic Flux Density B [T]	Load Resistance R_L [mΩ]	Load Voltage V_L [V]	Pressure Inlet P_{in} [psia]	Pressure Exit P_{out} [psia]	Power Output P_e [kW]	Average Void Fraction $\bar{\alpha}$
2-22-77	1	6.025	0	.584	.388	.234	44.3	33.5	.141	0
	2	5.98	.06453	.583	.400	.586	45.0	33.3	.897	.722
	3	9.127	.10111	.583	.399	1.022	57.0	32.3	2.618	.744
	4	10.566	.119694	.595	.400	1.235	64.0	31.1	3.813	.736
2-25-77	1	6.05	0	.587	.246	.225	46.4	34.7	.206	0
	2	6.02	.03318	.586	.253	.435	46.8	33.0	.748	.429
	3	9.08	.04934	.591	.251	.744	56.3	30.5	2.205	.566
	4	12.09	.068875	.587	.249	1.024	67.3	28.2	4.211	.564
	5	5.98	.01457	.591	.246	.359	46.6	32.7	.524	.352
	6	9.08	.020712	.591	.247	.555	53.7	31.2	1.247	.340
	7	12.09	.029687	.587	.247	.732	57.8	29.5	2.169	.370
	8	15.02	.034275	.586	.249	.897	64.8	27.3	3.231	.368
	9	18.12	.041297	.585	.247	1.075	70.3	23.2	4.679	.302
3-1-77	1	6.02	0	.583	.238	.223	45.6	34.2	.209	0
	2	9.04	0	.587	.240	.340	50.1	32.8	.482	0
	3	12.10	0	.587	.240	.452	55.3	32.9	.851	0
	4	15.06	0	.587	.223	.520	60.7	32.7	1.213	0
	5	18.17	0	.587	.242	.695	61.0	27.7	1.996	0
	6	21.13	0	.587	.242	.795	65.7	29.2	2.612	0
	7	6.02	.04136	.575	.248	.454	50.4	34.5	.833	.617
	8	9.13	.07252	.587	.218	.843	60.4	30.9	2.866	.680
	9	11.51	.10927	.587	.246	1.162	72.3	27.5	5.489	.678

Date	Run Number	Mass Flow Rate NaK $\dot{m}_\ell$ [kg/s]	Mass Flow Rate N_2 $\dot{m}_g$ [kg/s]	Magnetic Flux Density B [T]	Load Resistance R_L [mΩ]	Load Voltage V_L [V]	Pressure Inlet p_{in} [psia]	Pressure Exit p_{out} [psia]	Power Output P_e [kW]	Average Void Fraction $\bar{\alpha}$
3-1-77 (cont'd)	10	5.98	.07587	.585	.248	.520	48.0	32.2	1.090	.726
	11	9.04	.11356	.587	.246	.925	63.8	31.8	3.478	.735
	12	10.52	.12641	.587	.246	1.129	72.1	30.3	5.181	.713
	13	5.98	.05283	.597	.249	.542	48.8	31.1	1.180	.718
3-4-77	1	3.15	0	1.202	.239	.239	55.1	34.1	.237	0
	2	2.97	.00574	1.202	.246	.334	52.7	31.1	.221	.233
	3	3.04	.02365	1.201	.248	.369	54.8	32.7	.549	.372
	4	2.92	.02916	1.201	.249	.366	53.6	34.0	.538	.386
	5	2.83	.03538	1.201	.248	.390	55.6	33.1	.613	.408
	6	2.92	.05009	1.202	.250	.420	56.7	33.6	.706	.574
	7	3.04	.06357	1.2	.258	.444	56.8	32.9	.789	.616
	8	3.01	.12672	1.199	.249	.475	59.8	32.4	.906	.724
3-7-77	1	6.07	0	1.2	.238	.512	99.2	33.6	1.101	0
	2	6.025	.01483	1.2	.245	.729	93.7	31.2	2.169	.221
	3	6.025	.04230	1.2	.248	.826	91.6	33.1	2.751	.368
	4	6.025	.05205	1.2	.248	.857	89.3	33.0	2.961	.389
	5	5.98	.06614	1.2	.246	.885	89.2	31.8	3.184	.423
	6	5.98	.08570	1.2	.247	.920	81.5	33.0	3.428	.538
3-8-77	1	6.025	0	1.2	.380	.512	87.6	33.2	.703	0
	2	6.025	.02884	1.2	.392	.762	80.7	33.1	1.481	.293
	3	6.025	.03305	1.2	.394	.873	78.0	33.3	1.934	.429
	4	6.07	.04731	1.2	.392	.908	82.7	33.0	2.103	.436

Date	Run Number	Mass Flow Rate NaK $\dot{m}_\ell$ [kg/s]	Mass Flow Rate N_2 $\dot{m}_g$ [kg/s]	Magnetic Flux Density B [T]	Load Resistance R_L [mΩ]	Load Voltage V_L [V]	Pressure Inlet p_{in} [psia]	Pressure Exit p_{out} [psia]	Power Output P_e [kW]	Average Void Fraction $\bar{\alpha}$
3-10-77	1	5.98	0	1.2	.376	.507	88.7	34.0	.684	0
	2	6.025	.52308	1.2	.398	.928	75.5	32.2	2.164	.514
	3	6.00	.80765	1.2	.395	.980	78.6	31.0	2.431	.588
	4	6.025	0	1.6	.383	.655	106.0	30.2	1.120	0
	5	6.07	0	1.4	.381	.586	89.0	30.0	.901	0
	6	5.98	.01371	1.4	.394	.825	83.8	30.3	1.727	.241
	7	5.98	.03684	1.4	.397	.958	85.0	32.0	2.312	.409
	8	5.98	.05219	1.4	.396	.990	84.5	32.2	2.475	.446
3-11-77	1	6.025	0	1.4	.384	.589	92.4	34.6	.903	0
	2	6.00	.065868	1.4	.396	1.017	88.7	32.5	2.618	-
	3	6.07	.086773	1.4	.398	1.069	85.5	34.0	2.871	-
	4	5.98	0	1.4	.235	.576	103.7	33.0	1.412	0
	5	5.98	.014085	1.4	.249	.768	101.7	32.1	2.369	-
	6	6.025	.034776	1.4	.248	.910	104.5	33.0	3.340	-
	7	6.025	.056635	1.4	.250	.940	101.7	32.1	3.534	-
	8	5.98	.069453	1.4	.250	.948	100.6	32.1	3.595	-
3-17-77	1	6.025	0	1.235	.241	.468	78.8	34.1	.909	0
	2	6.07	.01382	1.235	.248	.652	78.8	33.3	1.714	.461
	3	5.98	.03342	1.205	.253	.749	79.0	34.2	2.188	.660
	4	6.07	.05023	1.205	.250	.785	78.2	33.4	2.465	-
	5	5.98	.06759	1.205	.253	.810	78.0	33.2	2.593	.623
	6	6.025	.05980	1.205	.249	.786	84.0	33.4	2.481	.349

Date	Run Number	Mass Flow Rate NaK $\dot{m}_x$ [kg/s]	Mass Flow Rate N_2 $\dot{m}_g$ [kg/s]	Magnetic Flux Density B [T]	Load Resistance R_L [mΩ]	Load Voltage V_L [V]	Pressure Inlet P_{in} [psia]	Pressure Exit P_{out} [psia]	Power Output P_e [kW]	Average Void Fraction α
3-17-77 (cont'd)	7	6.07	.04339	1.205	.248	.769	81.5	34.1	2.385	.396
	8	6.07	.03124	1.205	.248	.728	80.0	33.4	2.137	.392
	9	5.98	.07847	1.205	.250	.818	82.0	34.1	2.676	.563
3-18-77	1	6.025	0	1.203	.242	.460	78.5	33.2	.874	0
	2	5.98	.081485	1.207	.251	.825	77.8	32.2	2.701	.668
	3	5.98	.01414	1.207	.247	.619	82.8	34.0	1.551	.350
	4	12.09	0	.593	.382	.456	50.0	31.0	.544	0
	5	12.05	.03050	.491	.393	.711	51.7	28.2	1.286	.376
	6	12.23	.05924	.491	.393	1.007	60.8	32.7	2.580	.587

SECURITY CLASSIFICATION OF THIS PAGE *(When Data Entered)*

REPORT DOCUMENTATION PAGE

READ INSTRUCTIONS BEFORE COMPLETING FORM

1. REPORT NUMBER: ANL/MHD-78-2	2. GOVT ACCESSION NO.
3. RECIPIENT'S CATALOG NUMBER	
4. TITLE *(and Subtitle)*: EXPERIMENTAL TWO-PHASE LIQUID-METAL MAGNETOHYDRODYNAMIC GENERATOR PROGRAM	5. TYPE OF REPORT & PERIOD COVERED: Annual Report, October 1976 to September 1977
	6. PERFORMING ORG. REPORT NUMBER: ANL/MHD-78-2
7. AUTHOR(s): M. Petrick, G. Fabris, E. S. Pierson, A. K. Fischer, C. E. Johnson	8. CONTRACT OR GRANT NUMBER(s): N00014-77-F-0006
9. PERFORMING ORGANIZATION NAME AND ADDRESS: Argonne National Laboratory, 9700 South Cass Avenue, Argonne, Illinois 60439	10. PROGRAM ELEMENT, PROJECT, TASK AREA & WORK UNIT NUMBERS: Task No. NR099-404
11. CONTROLLING OFFICE NAME AND ADDRESS: Office of Naval Research (Code 473), Department of the Navy, Arlington, Virginia 22217	12. REPORT DATE: May 1978
	13. NUMBER OF PAGES: 95
14. MONITORING AGENCY NAME & ADDRESS *(if different from Controlling Office)*: Same as 11	15. SECURITY CLASS. *(of this report)*: Unclassified
	15a. DECLASSIFICATION/DOWNGRADING SCHEDULE

16. DISTRIBUTION STATEMENT *(of this Report)*

Approved for public release; distribution unlimited

17. DISTRIBUTION STATEMENT *(of the abstract entered in Block 20, if different from Report)*

18. SUPPLEMENTARY NOTES

19. KEY WORDS *(Continue on reverse side if necessary and identify by block number)*

armature reaction	load voltage	surfactants
bubble parameter	magnetohydrodynamics	two-phase
foams	pressure gradient	void fraction
generator efficiency	quality	
liquid metals	slip	

20. ABSTRACT *(Continue on reverse side if necessary and identify by block number)*

Testing of the second diverging-channel generator with the revised ambient-temperature NaK-N_2 facility has been completed. The primary goal of the revised facility, demonstrating reduced slip ratio (ratio of gas velocity to liquid velocity) with higher liquid velocity (flow rate), was accomplished. The reduction in slip ratio was dramatically demonstrated by a series of consecutive runs with varying flow rate (from 6 kg/s to 12 kg/s

DD FORM 1 JAN 73 1473 EDITION OF 1 NOV 65 IS OBSOLETE
S/N 0102-014-6601

SECURITY CLASSIFICATION OF THIS PAGE *(When Data Entered)*

20. Abstract (Cont'd)

for the liquid). Substantial increases in generator efficiency were obtained with higher liquid flow rates.

Experiments to demonstrate that good liquid-to-gas heat transfer exists in the generator were successfully completed. Good heat transfer is essential because it is the almost constant temperature expansion of the gas (vapor) in the generator that yields higher system efficiencies for liquid-metal MHD power cycles.

The feasibility of generating relatively-stable bubbles, hence, a foam, in liquid metals has been demonstrated. Photographic documentation of these phenomena, both motion and still pictures, was made. Surface tension measurements and foaming experiments have shown that viscosity is also a factor in promoting bubble formation and persistence. Wetting and contact angle measurements have been made for stainless steel and carbon steel immersed in eutectic NaK.

An analytical study of the liquid shunt (wall) layer sizes and losses has shown that these losses are not expected to be significant for large generators; less than 1.0% decrease in efficiency is anticipated. A two-phase pressure-gradient correlation developed for MHD flows has been shown to agree to within 20% with the generator data.

Distribution List For

Annual Report On

Liquid-Metal Magnetohydrodynamic Power

Activity	No. of Copies
Administrative Contracting Officer DCASO, Huntsville 2109 West Clinton Avenue Huntsville, Alabama 35805 Attn: Mr. D. W. VanBrunt	1
Office of Naval Research Department of the Navy Arlington, Virginia 22217 Attn: Mr. J. A. Satkowski, Code 473 Attn: Mr. B. Friedman, Code 221C	3 2
Commanding Officer Office of Naval Research Branch Office 536 South Clark Street Chicago, Illinois 60605	1
Director U.S. Naval Research Laboratory Washington, D.C. 20390 Attn: Code 2629 Attn: Code 2627	6 6
Defense Documentation Center Cameron Station Alexandria, Virginia 22314	12
Commander Naval Sea Systems Command Department of the Navy Washington, D.C. 20360 Attn: Dr. John Huth, Chief Scientist Attn: Mr. R. M. Forsell, Code 08	1 1
Commanding Officer Air Force Office of Scientific Research Bolling Air Force Base Building 41C Washington, D.C. 20332 Attn: Dr. B. Wolfson	1
Commander Naval Underwater Systems Center Fort Trumbull New London, Connecticut 06320 Attn: Technical Library	1

Activity	No. of Copies
General Electric Company Valley Forge Space Technology Center P.O. Box 8555 Philadelphia, Pennsylvania 19101 Attn: Dr. B. Zauderer	1
University of Maryland Department of Mechanical Engineering College Park, Maryland 20742 Attn: Dr. M. E. Talaat	1
Stanford University Department of Mechanical Engineering Stanford, California 94305 Attn: Professor R. H. Eustis	1
Rand Corporation 1700 South Main Street Santa Monica, California 90401 Attn: Technical Library	1
Jet Propulsion Laboratory 4800 Oak Grove Drive Pasadena, California 91103 Attn: Dr. D. G. Elliott	1
Energy Research and Development Administration Oak Ridge Operations Officer Reactor Division Oak Ridge, Tennessee 37830 Attn: Mr. J. Pidkowicz	1
University of Texas Department of Electrical Engineering Plasma Dynamics Research Laboratory Austin, Texas 78712 Attn: Dr. O. M. Friedrich, Jr.	1
Institute for Defense Analyses 400 Army-Navy Drive Arlington, Virginia 22202 Attn: Mr. R. Hamilton	1
Massachusetts Institute of Technology Department of Aeronautics and Astronautics Cambridge, Massachusetts 02139 Attn: Dr. J. Louis	1

Activity	No. of Copies
Los Alamos Scientific Laboratory P.O. Box 1664 Los Alamos, New Mexico 87544 Attn: Technical Library	1
Naval Surface Weapons Center Dahlgren, Virginia 22448 Attn: Technical Library	1
Superintendent U.S. Naval Postgraduate School Monterey, California 93940 Attn: Library, Code 0212	1
Commanding Officer Naval Ocean Research and Development Activity Bay St. Louis, Mississippi 39520 Attn: Technical Library	1
Officer in Charge Naval Ship Research and Development Laboratory Annapolis Division Annapolis, Maryland 21402 Attn: Special Projects Division Library, Code 421A	1 1
Commander Naval Weapons Center Propulsion Applied Research Group China Lake, California 93555 Attn: Technical Library	1
Air Force Aero Propulsion Laboratory AFAPL/POP-2 Wright Patterson Air Force Base, Ohio 45433 Attn: Mr. R. Cooper/55475	1
Commander Naval Surface Weapons Center White Oak Silver Spring, Maryland Attn: Technical Library	1
National Aeronautics and Space Administration Lewis Research Center 21000 Brookpark Road Cleveland, Ohio 44135 Attn: Dr. L. Nichols	1

Activity	No. of Copies
National Science Foundation Engineering Division Washington, D.C. 20550 Attn: Dr. Royal Rostenbach	1
Lawrence Livermore Laboratory Technical Information Department P.O. Box 808 Livermore, California 94550 Attn: Mr. H. Cheung Mr. O. Loper	 1 1
Commandant U.S. Marine Corps, Code CSY-3 Headquarters, Marine Corps Washington, D.C. 20380	1
North American Rockwell Atomics International P. O. Box 309 Canoga Park, California 91304 Attn: Mr. J. C. Cochran	 1
Knolls Atomic Power Laboratory Schenectady, New York 12301	1
Avco-Everett Research Laboratory 2385 Revere Beach Parkway Everett, Massachusetts 02149 Attn: Ray Janney	 1
University of Tennessee Space Institute Tullahoma, Tennessee 37388 Attn: Dr. J. B. Dicks	 1
Air Vehicle Corporation 8873 Balboa Avenue San Diego, California 92123 Attn: Dr. J. Rosciszewski	 1
STD Research Corporation P.O. Box C, Arcadia Pasadena, California 91106 Attn: Dr. J. C. Cutting	 1

Activity	No. of Copies
Cornell University Mechanical and Aerospace Engineering Ithaca, New York 14851 Attn: Professor E. Resler, Jr.	1
Case Institute of Technology Department of Electrical Engineering University Circle Cleveland, Ohio 44101 Attn: Dr. E. Reshotko	1
University of Pennsylvania Mechanical Engineering Department 335d and Locust Streets Philadelphia, Pennsylvania 19104 Attn: Dr. H. Yeh	1
California Institute of Technology 1201 East California Avenue Pasadena, California 91102 Attn: Technical Library	1
Colorado State University Department of Mechanical Engineering Fort Collins, Colorado 80521 Attn: Dr. H. E. Wilhelm	1
University of California Mechanical Engineering Department Davis, California 95616 Attn: Dr. M. Hoffman	1
Energy Research Corporation 15 Durant Avenue Bethel, Connecticut 06801 Attn: Technical Library	1
National Bureau of Standards U.S. Department of Commerce Boulder, Colorado 80302 Attn: Dr. Robert L. Powell	1
National Bureau of Standards U.S. Department of Commerce Washington, D.C. 20234 Attn: Dr. John Wachtman	1

Activity	No. of Copies
University of Florida College of Engineering 231 Aerospace Engineering Building Gainesville, Florida 32611 Attn: Dr. E. Rune Lindgren	1
Naval Material Command NAVMAT 0333 Washington, D.C. 20360 Attn: Mr. R. V. Vittucci	1
Defense Advanced Research Projects Agency 1400 Wilson Boulevard Arlington, Virginia 22209 Attn: Dr. George Donahue	1
Brown University Box D Providence, RI 02912 Attn: Dr. J. Kestin	1
The Rand Corporation 2100 M Street N.W. Washington, D. C. 20037 Attn: R. Y. Pei	1
U.S. Department of Energy MHD Program Office 20 Massachusetts Avenue Washington, D. C. 20545 Attn: M. Sluyter	1